Geomorphology 501 (2026) 110240

Contents lists available at ScienceDirect

Geomorphology

journal homepage: www.journals.elsevier.com/geomorphology

MARS modelling for spatial analysis of coastal erosion susceptibility

Grazia Azzara [a], Pietro Scala [b,*], Giorgio Manno [b,*], Francesco Raffa [c], Chiara Martinello [a], Antonio Tozzi [c], Edoardo Rotigliano [a], Giuseppe Ciraolo [b]

[a] Department of Earth and Marine Sciences (DiSTeM), University of Palermo, Via Archirafi 22, Palermo, 90123, Italy
[b] Department of Engineering (DI), University of Palermo, Viale delle Scienze, Building 8, Palermo, 90128, Italy
[c] Institute of Geosciences and Georesources, National Research Council (CNR-IGG), Via G. Moruzzi 1, Pisa, 56124, Italy

ARTICLE INFO

Keywords:
Coastal change analysis
Multivariate Adaptive Regression Splines
R-software
Shorelines Tuscany dynamics

ABSTRACT

This study assessed the susceptibility of the entire Tuscan coastline to coastal erosion using Multivariate Adaptive Regression Splines (MARS), a flexible yet interpretable non-parametric regression technique that explicitly models nonlinear relationships and variable interactions through physically meaningful thresholds. Unlike machine learning approaches commonly used in coastal erosion studies (e.g. SVMs, ANNs or logistic regression), MARS offers high predictive performance combined with enhanced transparency. This enables the controlling factors and their critical ranges to be interpreted more clearly. The coastline was segmented into transects spaced at 50 m intervals, and shore- line change was quantified for three periods (2000–2010, 2011–2020, and 2000–2020) using Net Shoreline Movement (NSM). To reduce uncertainty, two datasets were created: CUT2 (excluding transects with changes within ±2 m) and CUT4 (excluding those within ±4 m) according to shoreline digitalisation accuracy. The dependent variable was binarized to represent either eroding (1) or advancing (0) coastlines. The independent variables included coastal slope, number of storms, storm energy, depth of closure, geomorphology, and main longshore sediment transport directions, which are known to control coastal morpho dynamics at regional scale. Model calibration was conducted on 70% of the CUT4 dataset, with validation performed using both internal (30% of CUT4) and external (100% of CUT2) strategies. The performance of the MARS models was evaluated using ROC curves and AUC values, achieving good results (AUC $>$ 0.8) in most cases. The resulting susceptibility maps classified the coastline into four susceptibility levels (from low to very high) and showed strong agreement with observed shoreline trends. The identification of erosion hotspots was statistically supported by the MARS model outcomes and their associated variable contributions, while the relationship between persistently eroding sectors and limited sediment supply from river basins was derived from an integrated interpretation combining model results with geomorphological and observational evidence. Overall, the proposed MARS-based framework provides a robust, interpretable, and data-driven tool to support integrated coastal management, enabling the identification of critical erosion hotspots and the definition of targeted adaptation measures.

1. Introduction

Approximately 71% of the Earth's surface is covered by water, and the remaining 29% consists of land. The interaction between terrestrial and marine environment defines the coastline, which extends for about 1.6 km (Burke et al., 2001). Considering the ecological, economic, and social importance of coastal zone, Earth can be regarded as a coastal planet (Martínez et al., 2007).

The notable biological productivity and high accessibility make the coastal zone a magnet for human activity (Burke et al., 2001) hosting 40% of the world's population. The morphological action of rivers, currents and waves on sediments within the nearshore makes the coastlines complex and dynamic systems (Mentaschi et al., 2018) constantly changing, eroding and accreting. Due to climate change, sea-level rise and extreme events can accelerate the erosion process and cause potentially irreversible changes further intensified by human activity. The escalating frequency and intensity of the damage suggest that the coastal system is now less resilient and more vulnerable to extreme events (Intergovernmental Panel on Climate Change (IPCC; Stocker and Qin, 2013).

* Corresponding authors.
E-mail addresses: pietro.scala@unipa.it (P. Scala), giorgio.manno@unipa.it (G. Manno).

https://doi.org/10.1016/j.geomorph.2026.110240
Received 28 July 2025; Received in revised form 8 January 2026; Accepted 17 February 2026
Available online 20 February 2026

In the Mediterranean basin, these dynamics are particularly exacerbated due to the region's sensitivity to climatic pressures and intense anthropogenic alteration. In Italy, recent regional-scale studies have revealed critical challenges in sediment continuity and coastal retreat. An extensive satellite-based analysis covering the entire country over four decades (1984–2024) has shown that 66% of the 40 main Italian rivers are currently associated with erosion at their mouths, a value that reaches 100% when excluding stretches protected by hard coastal defences (Luppichini and Bini, 2025). This finding is symptomatic of a widespread sediment deficit in Italian river systems, largely driven by dam construction, land-use change, and reduced hydrological regimes (Luppichini et al., 2023).

Among the most critical areas identified at national level, several sectors along the Tuscan coast stand out for their persistent erosional trends. In particular, the deltas of the Arno and Ombrone rivers show long-term retreat rates that in some areas exceed 5–6 m per year (Besset et al., 2017; Bini, 2008; Cipriani et al., 2013). These trends are linked not only to reduced sediment delivery due to river regulation and upstream damming (Frangipane and Paris, 1994; Rinaldi, 2003), but also to climatic drivers such as decreased precipitation and increased frequency of extreme events (Baronetti et al., 2022; Blöschl et al., 2019). For example, the Arno basin has seen a progressive decline in annual discharge and sediment transport over the past century, particularly after the 1970s, reflecting broader hydrological shifts documented across the Mediterranean (Luppichini et al., 2024). In addition, to sediment supply reduction, coastal morphology in Tuscany is also shaped by longshore drift patterns and the interaction with human infrastructures. In the Pisa coastal plain, for instance, sediment dispersion analyses show that during high-discharge events, only a portion of the sediment plume reaches the adjacent coasts, while much of it is lost offshore due to morphological shadowing induced by harbour and jetty structures (Bini et al., 2021).

In view of these considerations, the assessment of the susceptibility/vulnerability of coastal areas to erosion is becoming a key global issue. A lot of techniques have been developed for this purpose, and they can be categorized into four main groups: a) Indicator-based approach (EUROSION, 2004); b) Index-based methods (e.g., the Coastal Vulnerability Index (CVI), Gornitz (1991)); c) GIS-based Decision Support Systems, and d) Complex system methods (e.g., Bayesian networks).

Indicator-based approaches express vulnerability of the coast through a set of independent indicators that reflect coastal issues, in contrast index-based approaches, combine different variables using weighting and ranking methodologies into a one-dimensional, risk/vulnerability index (Rangel-Buitrago and Anfuso, 2015; Tursi et al., 2025). Due to their relative simplicity, they are widely used for communication purposes. However, they also have some limitation; the index-based approaches are not immediately transparent, especially regarding the criteria used for ranking. Therefore, a clear explanation of the adopted methodology is essential to ensure their proper application.

The Decision Support Systems (e.g., DESYCO, Torresan et al. (2016)) integrate different types of information, powerful modelling functions, based on Multi-Criteria Decision Analysis (MCDA) in order to identify and prioritize areas and targets exposed to climate related hazard, estimate susceptible exposure units and relative risk. This methodology enhances the effectiveness of decision process in planning adaptation strategies but requires investment in terms of time and resources.

Finally, among the complex system methods are those based on Bayesian network (BNs) also known as Bayesian Belief Networks (BBNs). These are probabilistic graphical models which describe the relationships between a wider range of system's components (variables), by combining principles of Graph theory and probabilistic expressions (Pearl, 2001; Bayes, 1763). Gutierrez et al. (2011) used a Bayesian Network (BN) to integrate various factors - including relative sea level rise, wave height, tide range, coastal slope, geomorphology, and historical shoreline change- to predict long-term shoreline change to sea level rise along the U.S. Atlantic coast, demonstrating the effectiveness of BN approaches as predictive tools to support the decision-making process.

Other machine learning (ML) methods have been tested in the context of coastal hazard and vulnerability assessment. Park et al. (2019) implemented a Support Vector Machine (SVM) classifier to distinguish coastal zones using satellite images showing that although the model allowed a good identification of the coastline, its accuracy in detecting coastal changes remains limited. Park et al. (2019) assessed the future probability of coastal flooding events along the coastal area of South Corea, using six predictive variables and three ML algorithms - k-nearest neighbour (kNN), random forest (RF), and support vector machine (SVM) – demonstrating the potential of these data-driven models for coastal risk forecasting. Beuzen et al. (2019) proposed a probabilistic, data-driven approach using Gaussian Processes (GP) to generate ensemble predictions of wave run up demonstrating that integrating these GP machine learning models into coastal dune erosion models can improve forecast accuracy.

Despite the high predictive performance of ML methods, their “black-box” nature makes difficult to interpret the model's decision-making process, assess influence of individual variables, and detect potential biases or error. To overcome these limitations, this study used a Multivariate Adaptive Regression Splines (MARS) model (Friedman, 1991), to assess the natural susceptibility to coastal erosion along the entire coast of Tuscany. MARS is a non-parametric regression analysis technique capable of capturing complex and non-linear relationships between the dependent variable and independent variables without assuming a fixed functional form, offering greater flexibility than traditional linear regression techniques. The advantage of MARS lies in its interpretability and transparency. Unlike the black-box ML, the MARS approximations derive from an explicit mathematical expression of the output as a function on the input factors. Furthermore, MARS does not require arbitrary weighting of ranking of indicators like index- based methods which, although transparent, suffer from subjectivity.

The MARS methodology therefore represents an intermediate approach between the index-based methods and more complex probabilistic or Bayesian methods.

The primary aim of this research is to develop a reproducible an interpretable alternative to existing black-box models for assessing coastal erosion susceptibility, while minimizing the subjective assumptions typically associated with traditional index-based methods.

This research focused on the entire coast of Tuscany. Shoreline position data were collected for three time periods: 2000–2010, 2011–2020, and 2000–2020, and a preliminary analysis of coastal dynamic was conducted. To implement the MARS model, three changes inventories corresponding to each time period were prepared and used as dependent variables. A set of physical and environmental variables-assumed to influence shoreline dynamics-was selected as predictors. For each variable, a value was assigned to each transect (50 m equally spaced) in which the coastline was partitioned. For each time period, the dataset was split into two subsets, based on the resolution of the observed changes: $\pm$4 m (CUT4) and $\pm$ 2 m (CUT2), resulting in a total of six MARS models. Model performance was evaluated using the Area Under the Receiver Operating Characteristics Curve AUC. Finally, a susceptibility map was created and compared with the observed shoreline configurations.

2. Materials

2.1. Study area

The study area covers the entire coast of Tuscany (Fig. 1), excluding the islands. It is approximately 380 km long and includes open coastline as well as estuarine and deltaic sectors; the coast is mainly characterized by sandy beaches alternating with short segments of high and rocky coasts. The present morphological structure was formed in recent times (Quaternary), mainly due to the sediments deposited by the main rivers

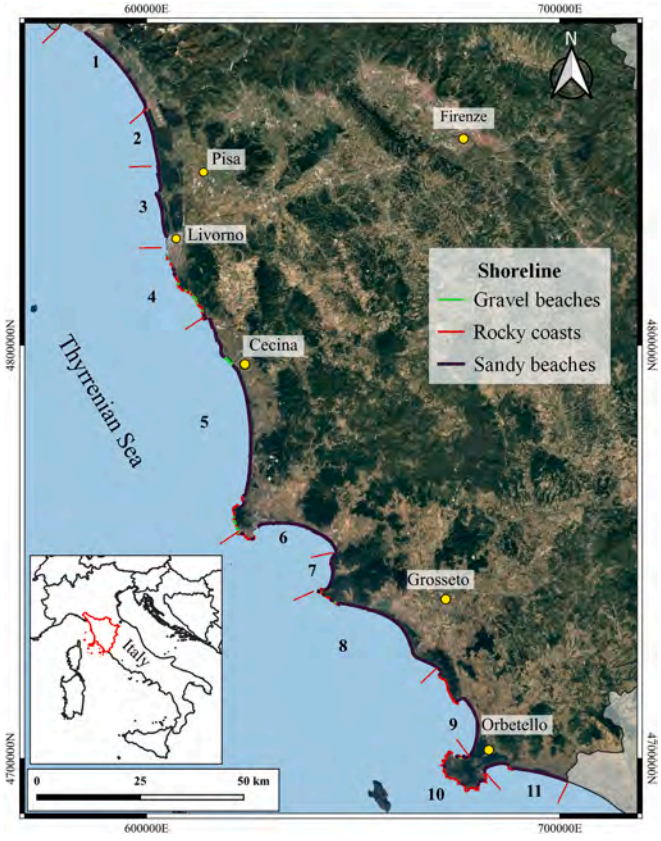

Fig. 1. Geographical setting and geomorphological characterization of the study area. The coastline classification, distinguishing between gravel beaches (green line), rocky coasts (red line), and sandy beaches (dark purple line). The coastline is subdivided into 11 Littoral Cells. Reference System: WGS84-UTM32N - EPSG:32632.

of Tuscany. The large coastal plain, stretching from Massa to Livorno, was formed by sediment input from the Arno and Magra rivers, which alone supply approximately 1,524,000 and 632,000 t / year of sediment, respectively (Pranzini et al., 2020). In addition to these, the Serchio 23,000 t / year (Cavazza, 1984) and the Frigido rivers also contributed to a lesser extent. The plains of Cecina, Follonica, and Grosseto were also formed in a similar way, with input from the Cecina, Cornia, and Ombrone rivers, respectively. In the southernmost part of the region, the coastal plains benefited not only from the input of the Tuscan rivers, but also from inputs from "outside the Tuscan region". In this case, the sediments transported northward are of volcanic origin, which gives rise to the beaches of Capalbio and Ansedonia. In some cases, along the Tuscan coast, low-energy environments generate lagoons and wetlands. The main wetlands are the Orbetello Lagoon, the Diaccia Botrona Marshes, and Lake Burano.

The Tuscan costs are highly critical from a geomorphological point of view, due to the anthropic activities that have taken place since the middle of the last century. Although the Tuscan coastline exhibits several geomorphological instabilities, it is not considered geologically critical because it is mostly composed of unconsolidated Quaternary deposits forming wide coastal plains, with limited occurrence of active rocky cliffs or structurally weak lithologies. The geological substrate does not undergo rapid mass wasting or tectonically driven retreat; instead, the observed changes are predominantly governed by sediment-budget dynamics, wave climate, and human interventions. For this reason, the coastal criticality in Tuscany is largely geomorphological, rather than geological. In the last 50 years, there has been a significant increase in the tourist, commercial and urban use of the coasts. This development has led to the need for coastal protection measures in various areas. These actions have involved the construction of marine structures and/or artificial beach nourishment. In an already greatly compromised situation, the failure of sediments to be delivered by rivers has been added, which has completely altered the natural deposition/erosion cycle. Recent studies on sedimentation along the coast, carried out through the application of new methodologies, highlight the dynamics of sediment deposition (Bini et al., 2021; Novi et al., 2022; Raffa et al., 2022). In addition, various research papers suggest that erosion of coastal areas adjacent to river mouths is mainly due to the reduction of sediment supply from rivers. However, shoreline retreat is often strongly influenced by the presence of offshore infrastructure, such as harbours and coastal defence structures. Analysis of the morphology of the seabed by Pranzini et al. (2020, 2018), taking into account both its slope and the presence of any submarine bars, shows a close correlation with shoreline evolution trends and the distribution of artificial structures. Bibliographic data also shows how regional-scale factors, such as wave energy and the presence of convergent or divergent sedimentary currents, significantly influence shoreline evolution. The longshore sediment transport distinguishes between sectors where currents converge and sectors where currents diverge. Convergent currents indicate zones where opposing longshore flows meet, promoting sediment deposition and favouring shoreline stability or accretion. In contrast, divergent currents correspond to sectors where longshore flows separate, producing net sediment export and enhancing the potential for erosion. This conceptual framework is commonly applied in Mediterranean coastal systems, where depositional nodes often coincide with convergence points and erosional hotspots with divergence zones. The adopted classification reflects these morphodynamic principles and aligns with the regional sediment budget described by Pranzini et al. (2020). The grain size characteristics of sediments on both the emerged and submerged beaches allow the identification of sediment transport vectors, both transverse and longitudinal, and the assessment of the impact of anthropogenic works on sediment flows. These analyses show how limited fluvial sediment inputs are and how erosion-prone beaches are the main sources of supply for the advancing coastal sections. Finally, the sedimentological study conducted in the recent past has made it possible to more accurately identify the zone of convergence of the littoral drift, where the granulometric characteristics of the sediments and the morphological characteristics of the seabed clearly differ from the coastal stretches dominated by a well-defined longitudinal flow.

2.2. Coastal changes inventories

To prepare the coastal changes inventories required for MARS modelling, the coastlines relative to the years 2000, 2010 and 2020 were used. The three shoreline datasets (2000,2010,2020) were selected to capture a 20-year evolution of the Tuscan coast, while the intermediate 2010 dataset enables assessing decadal-scale variability. To ensure temporal consistency, all three coastlines were extracted from imagery acquired during the summer period, thereby minimizing the influence of seasonal shoreline oscillations and avoiding the short-term morphological effects associated with winter storms. Summer acquisitions also reduce the likelihood of artefacts caused by adverse meteorological or sea-state conditions, such as cloud cover, wave run-up, or suspended sediment plumes.

The three coastlines (2000, 2010, 2020) were selected to ensure temporal consistency of both spatial resolution and acquisition period. The 2000 and 2020 coastlines originate from official ISPRA datasets (available on the website of the ISPRA at the following link: https://www.isprambiente.gov.it/it/banche-dati/banche-dati-folder/mare%20-%20last%20access%2013%20nov%202024), produced using the same photogrammetric workflow, while the 2010 coastline was derived from AGEA orthophotos with comparable 1 m resolution (https://www502.regione.toscana.it/geoscopio/ortofoto.html-lastaccess 13nov2024). All datasets were referenced to the same projection (WGS84–UTM 32 N), ensuring that differences among years are

attributable to real shoreline variations rather than methodological inconsistencies. The 2010 shoreline was digitalised automatically using the automatic coastline extraction model proposed by Scala et al. (2024a). This model exploits a Convolutional Neural Network architecture (CNN) that performs multiclass semantic segmentation (water, beach/sand, built-up, vegetation, bare land), enabling shoreline extraction as the boundary between the water class and all remaining classes. The model incorporates a Sobel-edge loss term that enhances its ability to detect transition zones. Validation on the San Leone case study (11 km of coast) shows that 80% of transects deviate less than 1 m from the ground truth, and that the model achieves an 85% goodness-of-fit when adopting a 2-m geometric accuracy threshold. Lower performance is observed in areas characterized by darker terrain or shadows, but overall, the method proves robust across sandy beaches, cliffs, and highly urbanized sectors. The shoreline extracted from the CNN output is obtained through a structured post-processing sequence composed of: (i) global thresholding of the semantic-segmentation raster, (ii) conversion to unsigned bytes, (iii) mean blurring using a 5-pixel kernel to reduce local artefacts, (iv) binary thresholding, and (v) cropping using a 50-m buffer to isolate the land–water transition. Finally, the coastline is defined as the isoline corresponding to the selected threshold level, ensuring a smooth representation of the natural boundary rather than a pixel-based discontinuous edge.

The coastlines were used as input to the CDA tool (Scala et al., 2024a, 2024b) to perform Transect-Based Analysis of coastlines. Using transects with an average inter-distance of 50 m, it was possible to obtain for the entire Tuscany coastline, the statistical indices of coastal changes EPR (End Point Rate), NSM (Net Shoreline Movement), SCE (Shoreline Change Envelope) and LRR (Linear Regression Rate). Although the CDA tool provides multiple indices, the MARS models were based on NSM values only. LRR was excluded because regression-based metrics are not robust when derived from only three shoreline positions. Likewise, EPR conveys the same information as NSM, as it represents its rate-based transformation. SCE was not considered representative for this study because it merely expresses the distance between the most landward and seaward shoreline for each transect; with only two shorelines available per analysed period, SCE would simply replicate NSM values without providing additional or significant insight. For these reasons, NSM was retained as the sole response variable for the modelling.

The observed Net Shoreline Movements were then used to create three coastal changes inventories for each reference period (2000–2010, 2011–2020, 2000–2020 - it should be specified that the notation 2011–2020 is used to differentiate it from the first time period, but the reference coastline is still 2010). Each transect was then assigned to one of the eleven littoral cells identified along the Tuscan coastline. A littoral cell is defined as a coastal segment where is assumed a limited sediment movement (Fig. 1). In detail, the sediment transferred from one littoral cell to its neighbouring littoral cells is here assumed as null or negligible. The littoral cells are identified based on several factors that determine sediment transport, such as, i) the shape of the coastline based on aerial/satellite imagery and bathymetric surveys; ii) the exposure of the area to waves; iii) the location of the river mouths; iv) the lithological features of the bedrock and sediments. For example, the evolutionary forms of river mouths, as well as accumulation and erosion close to coastal structures, highlight the prevalence of sediment flow in one direction; the cusps highlight a divergence of the flow; large concave steps highlight the continuity of the littoral cell (Pranzini and Williams, 2021).

Finally, to account for potential digitization errors in shadowed or geo-morphologically complex areas such as cliff-dominated settings, rocky coast transects were excluded from the MARS modelling to avoid introducing uncertainties that could compromise the reliability of the dataset. Moreover, those transects showing absolute variations of less than 2 m were excluded from the datasets and two subsets were so created: CUT2, which includes transects exhibiting shoreline absolute variations greater than 2 m and a more conservative dataset CUT4, which includes only transects with absolute variations greater than 4 m. In fact, based on the analysis of shoreline position variations along transects, under the assumption of morphological stability (i.e., absence of real shoreline advances or retreat), an average offset of 4 m was consistently observed. Therefore, this value was adopted as a conservative estimate of total positional uncertainty due to digitization errors.

3. Methods

In this research, coastal erosion susceptibility was evaluated by defining the relationships existing between a set of independent explanatory variables or predictors and the dependent variable, representing the outcome status to be predicted. The predictors are selected among those physical and environmental variables affecting the coastal erosion process and assigned to each of the mapping units in which the study area is partitioned. The dependent variable is the coastal change status extracted from the analysis of the coastlines related to different years and expressed as eroding or advancing coast (the outcome). Continuous NSM values were not used as dependent variable because shoreline position is affected by uncertainty, seasonal oscillations, and extreme-event variability. Binarizing the variable (erosion vs. accretion) reduces noise and enhances the ability of the MARS algorithm to detect robust relationships between predictors and dominant shoreline trends, which is common in susceptibility mapping applications. Among the wide fan of stochastic approaches suitable for setting functional dependence between predictors and outcome, multivariate adaptive regression splines (MARS, Friedman (1991)) have recently more and more adopted in facing environmental processes modelling (Conoscenti et al., 2018; Martinello et al., 2022, 2023; Mercurio et al., 2021).

3.1. The MARS method

MARS is a non-parametric regression technique which identifies non-linear adaptation relationships between independent and dependent variables. In particular, MARS divides the range of the predictor values into windows, delimited by nodes (k), and generates a linear regression equation (“basis function”, BF) for each window, according to Eq. 1:

$$y = a + \sum_{n=1}^{N} \beta_n h_n(x_n) \quad (1)$$

where: y is the target variable; α is a constant; N is the number of terms, each formed by a coefficient β_n; and $h_n(x)$ is a single BF or a product of two or more BFs of the independent variable x. The individual BF has the form max (0, x - κ) or max (0, κ - x), where x is an explanatory variable and κ is a constant corresponding to a knot.

In this study, the dependent variable was binarized assigning a value of 1 or 0 to transects exhibiting shoreline erosion or accretion, respectively. In the context of susceptibility maps, it is common practice to use binary classification for the dependent variable to classify the areas potentially susceptible to a given process, this making clearer the interpretation of the model outputs, especially from the perspective of hazard mitigation and management. Additionally, shoreline positioning is often affected by uncertainty such as measurement errors, seasonal variations, and long-term natural cycles and simplifying the observed data into binary categories, allow us to reduce the uncertainties and stresses the main trend (erosion vs. advancement). Finally, binary classification enables the applications of robust metrics for validation, such as accuracy, precision, recall, and AUC-ROC curve.

3.2. Predictors

In order to produce the coastal susceptibility map of Tuscany, six physical coastal variables were selected, in light of their role in coastal erosion processes, including: geology and geomorphology (G), coastal slope (S), the number and energy of storms (S_t and W_e, respectively), the distance of the closure depth from the coastline (h_c), and the main

longshore transport directions (D_r) (Table 1). The choice of the six predictors used in the MARS modelling was based on a combination of physical relevance, data consistency, preliminary statistical testing, and expert knowledge of coastal dynamics. The selected indicators represent the main components controlling shoreline mobility along the Tuscan coast and were grouped into three thematic categories: a) Coastal intrinsic characteristics (G, S); b) Marine forcing (S_t, W_e, h_c); and c) Sediment transport dynamics (D_r). The selected variables also meet practical criteria: they are spatially continuous, available for the entire coastline, and derived from authoritative and repeatable datasets, ensuring reproducibility and applicability to other regions. S_t and W_e were calculated at the littoral cell scale and then assigned to each transect within the corresponding cell, while S, h_c, G and D_r were computed individually for each transect. As a result, the values of the indicators calculated per transect vary from transect to transect, whereas the values of indicators computed at the littoral cell scale are identical for all transects belonging to the same cell. This method assumes that the wave climate factors represented by S_t and W_e remain spatially uniform across the transects.

3.2.1. Geomorphology (G)

The geomorphological and geological characteristics of the coastal sector were derived from the ISPRA (Istituto Superiore per la Protezione e la Ricerca Ambientale) Coastal Geo- portal by intersecting each coastal transect with the two vector-based shoreline datasets (corresponding to the years 2000 and 2020) and assigning the local properties to their centroid. Besides, the "Carta della Natura" map was analysed, which represents habitats and biotopes as defined by the CORINE Biotopes System (provided by the regional geo-information system - https://www.regione.toscana.it/-/geoscopio-lastaccess13nov2024), to discriminate two specific habitats: embryonic shifting dunes (16.21 CORINE biotopes) and fixed coastal dunes with herbaceous vegetation (16.22 CORINE biotopes). In fact, the presence of these habitats in the back-shore areas of low sandy coasts could enhance the resilience and reduce the vulnerability of these coastal areas. The final adopted classes used are listed in Table 2. As mentioned in the section 2.2 high and low rocky coasts were excluded.

3.2.2. Coastal slopes (S)

The slope of the subaerial coastal plain was extracted from a digital terrain model (DEM) with a spatial resolution of 2 meters, provided by the regional geo-information system. In particular, the average slope within a 25-m radius was obtained for each transect and assigned to its centroid.

3.2.3. Sea storms (S_t)

The specific dataset provided by CMEMS, known as MEDSEA MULTIYEAR WAV 006012, was used to analyse wave climate along the Tuscan coast. Key parameters extracted include significant wave height (H_{m0}), spectral peak period (T_p), and mean wave direction (θ), calculated using wind data provided by the European Centre for Medium-Range Weather Forecasts (ECMWF), with a spatial resolution of 0.5° × 0.5°. Fig. 2 shows the CMEMS data collection points around the Tuscan coast for each Littoral Cell.

Table 1
List of predictors.

Variable		Data source	Units	Reference year
CONTINUOUS				
S	Coastal slope	DEM 2 × 2 m	%	
S_t	Number of storms	CMEMS	–	2000–2010 / 2011–2020
W_e	Storm Energy	CMEMS	kW/m	2000–2010 / 2011–2020
h_c	Depth of closure	CMEMS	m	2000–2010 / 2011–2020
CATEGORICAL				
G	Geomorphology	ISPRA	–	2000/2020
D_r	Main longshore transport directions	Pranzini et al., 2020	–	2020

Table 2
Categorical classification of geomorphological and habitat types for MARS modelling.

Geomorphology + habitat	Class of variable
Low gravelly coast	**1**
Low sandy coast	**2**
Low sandy coast + shifting dunes or fixed coastal dunes with herbaceous vegetation	**3**
Connections	**4**
Coastal defence structure	**5**
Riverbanks	**6**

Wave climate along the Tuscany coast was analysed for the time interval covered by the study. 55 points were selected from the CMEMS reanalysis dataset (as shown in Fig. 2). The representative parameters for each coastal stretch are wave height H_{m0}, period T_p, and mean direction θ. These spatially distributed parameters of the selected points were used to define the wave climate for each coastal cell. These wave climate parameters were then used to calculate in MATLAB both storm event and energy flux predictors, related to marine climate. Among the indicators considered were the number of storms, average annual maxima of energy flux, and depth of closure (d_c). For each temporal window (2000–2010 and 2011–2020), all storm events are considered, with a storm defined following Boccotti (2000) as $H_{m0} > 1.5$ m sustained for more than 12 consecutive hours. Events separated by more than 12 h below this threshold are considered independent. The mean storm energy over the window is calculated as a weighted average of annual mean energies, with weights proportional to the number of storms per year.

In this context, a storm in the Mediterranean Sea has been defined as a series of sea states in which the spectral significant wave height (H_{m0}) exceeds 1.5 m and remains above this value for a continuous period of more than 12 h. If more than 12 h have elapsed between one exceedance of the 1.5 m threshold and the next, then the storms are considered independent, vice versa the sea storm is considered unique. The number of storm surges recorded for the periods 2000–2010, 2010–2020, and 2000–2020 was calculated for each littoral cell (Table 3).

The total energy (E) of each storm surge, which provides an indication of the potential hazard that the storm surge exerts on the coastal zone, following the methodology adopted by Mendoza and Jiménez (2005), was calculated by integrating the significant wave height for the duration of the event (t_1, t_2):

$$E = \int_{t_1}^{t_2} H_s^2 \, dt \tag{2}$$

From the total energy, it was possible to calculate wave energy flux, a crucial factor in assessing coastal vulnerability. To consider its variations, the average of annual maxima was calculated. For each year and for each littoral cell, the maximum wave energy flux (P) value (Eq. 3) was determined from the wave energy values. These maximum values were then averaged over time to obtain a single value for each cell for the three different time intervals.

$$P = E \bullet C_g \tag{3}$$

where C_g is the group celerity. Storm energy flux values were used in their original units (kW/m). No logarithmic or standardizing transformation was applied, since the variable's magnitude directly reflects physical wave forcing intensity, and preliminary tests confirmed that MARS effectively handled the numerical range without requiring scaling.

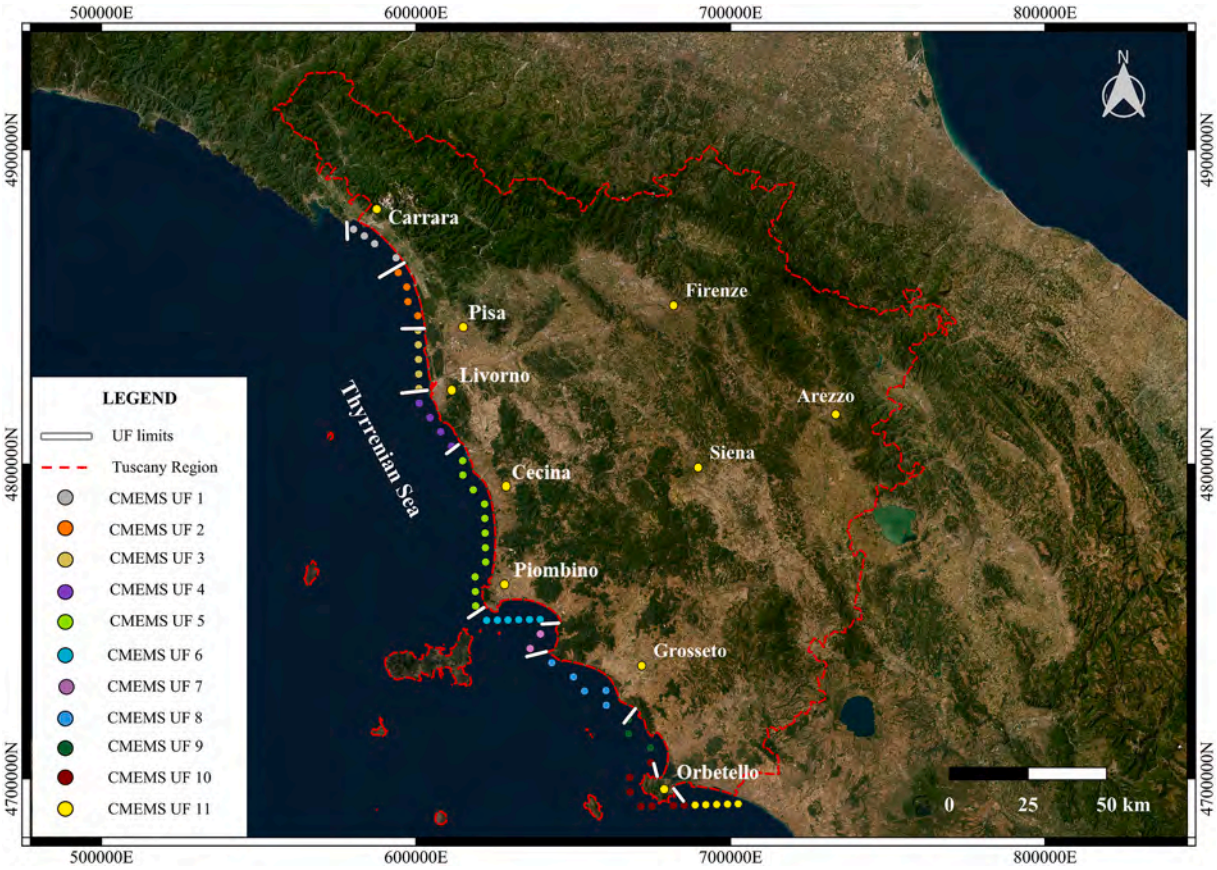

Fig. 2. CMEMS wave data point along Tuscany region used. Reference System: WGS84-UTM32N - EPSG:32632.

Table 3
Storm energy flux, number of detected storms and h_c for each littoral cells.

Littoral cell	2000–2010			2011–2020		
	N° of storms	Energy flux *[kW/m]*	h_c *[m]*	N° of storms	Energy flux *[kW/m]*	h_c *[m]*
1	194	140.4	7.58	179	157.27	8.02
2	189	132.10	7.42	173	150.61	7.93
3	235	148.11	7.82	210	175.99	8.53
4	255	147.06	7.80	221	180.58	8.64
5	309	114.48	6.88	292	146.30	7.78
6	296	112.57	6.82	285	128.39	7.28
7	130	106.70	6.64	130	125.16	7.19
8	258	103.96	6.55	248	122.20	7.11
9	171	88.54	6.05	167	107.64	6.67
10	240	141.99	7.66	220	158.21	8.09
11	223	133.20	7.42	208	140.49	7.62

3.2.4. *Depth of closure (h_c)*

For each CMEMS point located near the coast, the depth of closure was also calculated using Hallermeier's formula (h_c) which allows estimating the depth beyond which marine sediment transport is insignificant during normal sea conditions. The depth of closure (h_c) represents the offshore boundary beyond which cross-shore sediment transport becomes negligible. It is physically linked to sediment budget dynamics and wave energy exceedance statistics. Therefore, hc reflects the long-term morphodynamic domain actively contributing to shoreline adjustment. The depth of closure was calculated using Eq. 4.

$$h_c = 2.28\, H_{s_{12}} - 68.5\left(\frac{H_{s_{12}}^2}{g\, T_{12}^2}\right) \quad (4)$$

where $H_{s_{12}}$ is the significant wave height exceeded 12 h per year (i.e., the wave height with a yearly exceedance probability of 0.137%), T_{12} is the period associated with H_{s12}, and g is the gravitational acceleration (m/s^2).

This calculation was performed on an annual basis for each point, then averaging the results obtained for the various time intervals considered in the study. The depth of closure values obtained for each point in the CMEMS network made it possible to extract from EMODnet (European Marine Observation and Data Network - https://emodnet.ec.europa.eu/en/bathymetry – last access 13 Nov 2024) bathymetry for the Tuscany area, the corresponding bathymetric lines so as to obtain curves at fixed depth of closure for each time period (Fig. 3). Bathymetric data processing and extraction of closure-depth contours were carried out in QGIS. The inclusion of the depth of closure in the analyses allowed for a more complete and detailed characterization of marine conditions along the Tuscan coast, providing additional data for coastal vulnerability assessment and integrated coastal zone management. Results on the number of storms, energy flux and hc for each UF and for each period are presented in Table 3.

3.2.5. *Long-shore current (D_r)*

To incorporate the information on the main longshore transportation, the prevailing directions of the currents along the Tuscany coast, as reported in the study by Pranzini et al. (2020) were used. In particular, to discriminate between areas of erosion (i.e. where opposite current flows end) and deposition (where two opposite streams meet), a classification system with four classes was adopted, from class 1, identifying transects where currents converge, to class 4, where currents diverge. Empirically, the divergent sector can be view as 'sediment source', where hydrodynamic condition removes sediment toward onshore sector, creating a sediment deficit. Classes 2 and 3 identify transitional zones that connect divergence and convergence zones, classified based on their spatial position to the divergence or

Fig. 3. Depth of closure along Tuscany region. Reference System: WGS84-UTM32N - EPSG:32632.

convergence zones. The convergence zone is a sector that acts as sediment sink, favouring the deposition.

3.3. Calibration and validation sampling strategy

As described in Section 2.2 a total of three datasets were assembled from the full database, referring to three time periods: 2000–2010, 2011–2020 and 2000–2020. Besides, in order to check any effects in the model performance induced by more severe than 2 m spatial resolution limits in shoreline picking, two suites of models were prepared: CUT2, which excludes transects with shoreline changes between −2 and + 2 m, and CUT4, which excludes transects with variations between −4 and + 4 m. The total number of shorelines transects included in each dataset for the CUT2 and CUT4 is reported in Table 4.

Each MARS modelling procedure assumed the six predictors as explanatory variables and a binarized outcome (each transect was classified as 1, for retreatment and 0, for advancement). In particular, once the 0/1 status of a set of calibrating transect is given as input, the MARS modelling produces an estimate of the probability (score between 0 and 1) for any unknown validation transect to be in retreating (1) or advancing (0) status. The only requirement is that the values assumed by the explanatory variable in all the transects must be known.

Before proceeding with the modelling, each dataset was analysed to evaluate the ability of each single predictor to discriminate between retreating from advancing transects. To this aim, the Mann-Whitney Wilcoxon test was used for continuous and ordinal predictors, and the Chi-Squared test of Independence for the categorical variable. The resulting *p*-values (reported in Table 5) confirmed that, for most variables, the predictor distribution observed in retreating transects differs significantly from that observed in advancing transects ($p\text{-value} < 0.05$).

However, in some cases – such as variable W_e for the 2000–2020 dataset, h_c for 2011–2020 and G for 2011–2020 - the difference was not statistically significant. Although these results, they were retained due to their importance in coastal processes, and because the multivariate modelling is able to capture complex interaction and non-linear relationships which may not emerge from univariate analyses. Subsequentially, to explore any potential autocorrelation between the predictors, the variance inflation factor (VIF) was calculated, and a threshold VIF value of 10 was set to exclude collinear variables from the models. The result showed a moderate correlation between predictor variables (Table 6), so that all the variables were included in the modelling procedure.

Once the pre-exploring of the explanatory variables was performed,

Table 4
Total number of transects included in each dataset (2000–2020, 2011–2020, and 2000–2020) for the two model suites CUT2 and CUT4.

Dataset	N° of transects CUT2	N° of transects CUT4
2000–2010	3223	2659
2011–2020	3136	2544
2000–2020	3368	2792

Table 5
Results of the univariate analysis. The values shown the p-values obtained from Mann-Whitney-Wilcoxon Test (continuous/ordinal variables) and the Chi-Squared Test (categorical variable).

Test	Variable	2000–2010	2011–2020	2000–2020
Mann-	S	$< 2.2 \times 10^{-16}$	3.93×10^{-7}	$< 2.2 \times 10^{-16}$
Whitney-	S_t	3.51×10^{-6}	$< 2.2 \times 10^{-16}$	$< 2.2 \times 10^{-16}$
Wilcoxon	W_e	2.23×10^{-6}	9.84×10^{-8}	0.47
	h_c	$< 2.2 \times 10^{-16}$	0.151	$< 2.2 \times 10^{-16}$
	D_r	$< 2.2 \times 10^{-16}$	$< 2.2 \times 10^{-16}$	$< 2.2 \times 10^{-16}$
Chi-Square	G	$< 2.2 \times 10^{-16}$	0.2464	$< 2.2 \times 10^{-16}$

Table 6
Variance Inflation Factor (VIF) values for each variable across three-time dataset. All VIF values are very close to 1 and well below the common critical threshold (10), this confirms the absence of multicollinearity among the predictors.

Variable	2000–2010	2011–2020	2000–2020
S	1.08	1.05	1.09
S_t	1.15	1.12	1.13
W_e	1.15	1.21	1.16
G	1.03	1.02	1.03
h_c	1.10	1.14	1.13
D_r	1.07	1.06	1.08

MARS modelling was so implemented for the CUT4 dataset in the three periods: 2000–2010, 2011–2020, and 2000–2020 (Table 7). Each model was submitted to a validation procedure by applying a random partition strategy scheme, splitting into two balanced (retreating/advancing transects) calibration (70%) and validation (30%) subsets. Each random splitting was replicated one-hundred times so to check also the reliability of the results and the robustness of the modelling procedure. Besides, in order to verify the actual resolution of the CUT4 models, a validation on the entire CUT2 dataset was also performed. A total of six models was finally set for modelling (Table 7).

The prediction skill of the MARS models was estimated by calculating the area under the receiver operating characteristics curve (AUC; Lasko et al., 2005). An ROC curve plots the area under (AUC) the true positive rate (sensitivity) versus the false positive rate (1- specificity) at any given cut-off score. AUC values close to 0.5 indicate no ability of the model to discriminate between the levels of the target variable (0 = advancing, 1 = retreating), whereas AUC values equal to 1 represents perfect discrimination. Intermediate AUC values were interpreted, according to Hosmer et al. (2013) as acceptable, excellent and outstanding when AUC is higher than 0.7, 0.8 and 0.9, respectively. At the same time, the probabilities predicted from the one-hundred model replicates were averaged and binarized by applying a Youden index optimized cut-off (Youden, 1950), so that, by comparing the predicted to the observed status of each transect a confusion matrix was obtained and the numbers of true positives (TP), true negatives (TF), false positives (FP) and false negatives (FN) estimated.

4. Results

4.1. Shoreline change (2000−2020)

The spatial and temporal changes along the coastlines under study for the entire Tuscan region are illustrated in Fig. 4, which provides a detailed representation of coastal dynamics in terms of erosion and accretion transects for the periods 2000–2010, 2011–2020, and the overall period 2000–2020, respectively. The maps highlight six classes of shoreline change, expressed in meters, and colour-coded from intense erosion (down to -190 m, in dark red) to marked accretion (up to +116 m, in dark green). The analysis is accompanied by two detailed boxes (A1-C1 and A2-C2) that illustrate contrasting behaviours within the same UF: one area with predominantly shoreline advancement (near Viareggio) and another with retreat (north of Pisa), exemplifying sediment transfer between sub-sections. In the first period (2000−2010), a prevailing erosional regime is observed, with about 35% of the shorelines falling in the class of greatest retreat (-190 / -12.5 m). The southern sectors, particularly in the area highlighted in Box A2, show widespread erosion, suggesting marked morphodynamic instability, probably related to persistent sedimentary deficits and lack of effective fluvial input. Areas under accretion are very limited, with less than 5% of the stretches classified in the category of greatest advance (+9.2 / +116 m), mainly located at anthropogenic interventions or in areas of natural accumulation.

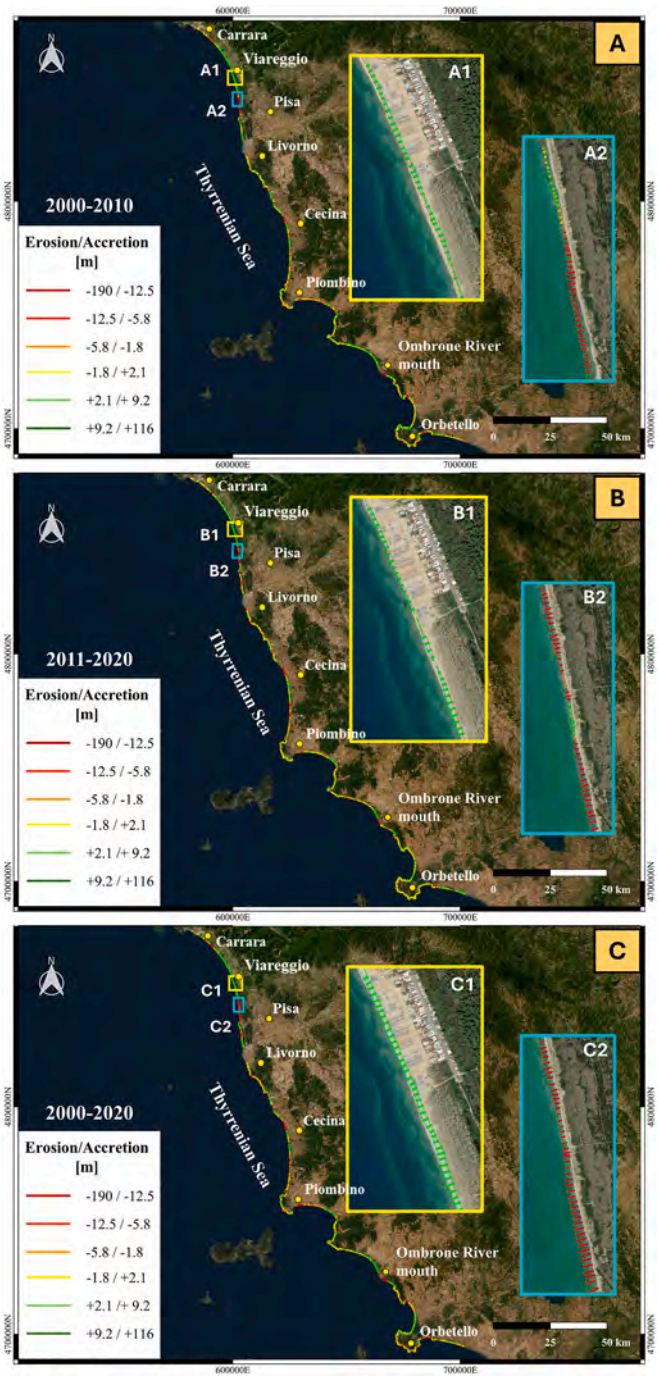

Fig. 4. Tuscany coastlines used for the analysis. Zoom areas are presented in the figure. Reference System: WGS84-UTM32N - EPSG:32632.

Table 7
Overview of calibration and validation strategies for models A–F across different temporal datasets (2000–2010, 2011–2020, and 2000–2020). Models were trained using 70% of dataset CUT4 and validated on the remaining 30% of CUT4 or validated using the full 100% CUT2 dataset.

Dataset	Calibration	Validation	Replicates	Model
2000–2010	70% CUT4	30% CUT4	100	A
		100% CUT2		B
2011–2020	70% CUT4	30% CUT4	100	C
		100% CUT2		D
2000–2020	70% CUT4	30% CUT4	100	E
		100% CUT2		F

In the subsequent period (2011−2020), the general picture appears to have partially changed. The extent of some erosional classes decreases (from about 35% to 30 per- cent), while the areas classified as stable (-1.8 / +2.1 m) or slightly accreting (+2.1 / +9.2 m) increase, reaching about 30% of the total overall. However, Box B2 highlights a reversal of the previous trend along the northern section, where portions of the shoreline that were previously stable or undergoing slight accretion are now affected by erosion. It is important to note that many of the areas previously characterized by erosion continue to show signs of retreat even in the second time interval, and in some cases with greater intensity than in the previous decade. In the cumulative period 2000–2020, the dynamics are the product of the combination of the previous two phases. There is a partial attenuation of the extreme erosional signals recorded in the first decade, but some critical hotspots persist, particularly in the Box C2, where retreats greater than -12.5 m continue to be recorded.

Finally, to assess the coastline dynamics between the two distinct observation periods for each littoral cell, the percentage of cases with coherent behaviour, i.e. with persistent advance or retreat in both periods, and the percentage of incoherent cases, characterized by a trend reversal (e.g. from advance to retreat, or vice versa) was quantified. Littoral Cells 4 and 10 were excluded from this analysis, as they are mostly characterized by rocky transects, which were omitted from the modelling as described in section 2.2. The percentage distribution of the transects in four morphodynamic categories – Advance, Retreat, Advance- Retreat and Retreat-Advance – highlights (Fig. 5) a substantial spatial heterogeneity. In particular, cells 3, 5 and 6 are dominated by a constant retreat, indicative of persistent erosive conditions. Conversely, only cells 1 and 2 show a significant percentage of transects with constant advancement. With regard to trend reversals, the littoral cell 8 shows the highest percentage of transects that went from advancement to retreat, followed by 7, 9 and 11 cells, where the opposite trend, i.e. from retreat to advancement, is more marked.

4.2. *Performance and predictive structure of MARS models*

The performance of the MARS models can be estimated in the cut-off independent domain of the ROC -plots where the results of one-hundreds models are averaged (Fig. 6). The results obtained attest for satisfactory to excellent performance for all the models, with CUT4 models showing an only slightly (2,5–3%) higher performance (Table 8). Besides, CUT4 model results are affected by a greater variability (larger IQR), as a consequence of the associated reduced sample size (more than five hundreds transects less on average, through the three time periods). At the same time, more similar conditions are expected to explain lower (±2 m) transect responses, so that more homogeneous calibration and validation subsets are obtained for CUT2 models.

The above described difference in the predictive performance seems to be associated with a different inner structure of the predictive models as attested by the Variable Importance analysis, showing the number of extraction of the potential predictors out of the one-hundred replicates of the three (A: 2000–2010, C: 2011–2020 and E: 2000–2020) CUT4 models (Fig. 7).

In general, coastal slope (*S*), class 4 of the main longshore sediment transport direction (D_r4), number of storms (S_t), storm energy (*We*) and the distance from depth of closure (h_c) resulted as the main controlling factors of the coast response. A secondary role (less than 25% of extractions) is assigned to the geomorphological setting of the coastal sectors with Low Sandy Coast, Connection and Riverbanks classes, mostly visible in the first decade (Fig. 7, green bars). The selection of coastal slope and distance to the depth of closure as primary predictors highlights the physical controls on shoreline evolution. A steeper slope generally corresponds to a reflective morphodynamic state, which is

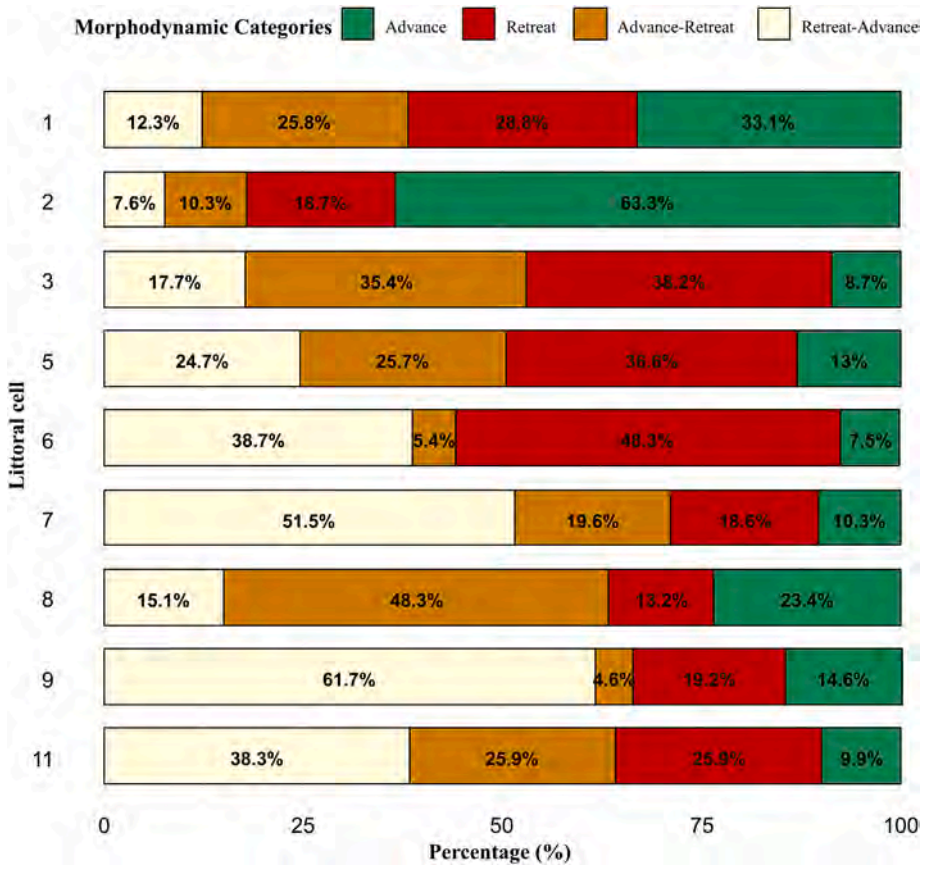

Fig. 5. Percentage distribution of transects within each littoral cell categorized by morphodynamic behaviour across two observation periods: constant advance, constant retreat, advance to retreat, and retreat to advance.

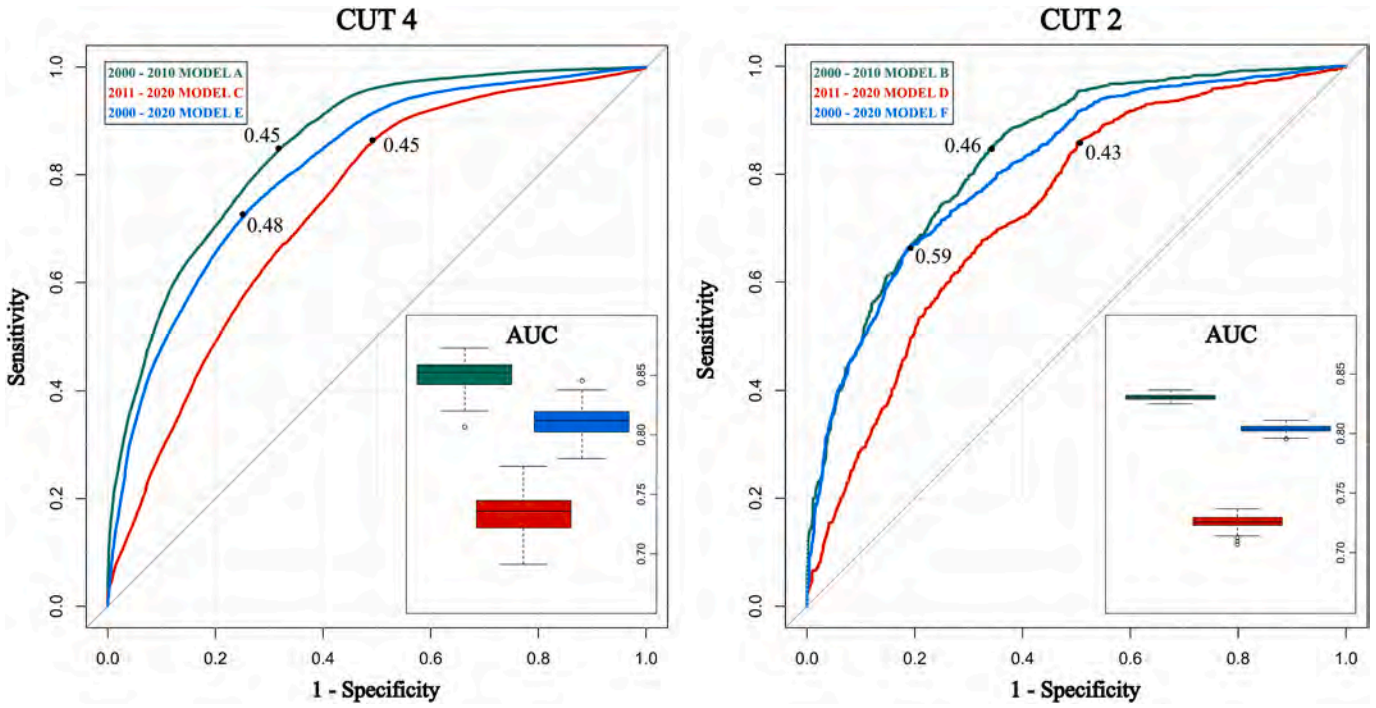

Fig. 6. Receiver Operating Characteristic (ROC) curves and corresponding AUC distributions for the MARS susceptibility models of the two datasets (CUT 4 and CUT 2). The ROC curves represent the average performance of 100 model replicates per configuration. The boxplots summarise the distribution of AUC values. The labelled points along the ROC curves indicate the optimal thresholds identified using the Youden Index criterion.

Table 8
Mean, minimum, maximum, SD and 95% CI AUC values for MARS models across three periods: 2000–2010 (Models A, B), 2011–2020 (C, D), and 2000–2020 (E, F).

Period	Model	Mean	Min-Max	SD	95% CI
2000–2010	A	0.85	0.80–0.87	0.01	0.847–0.852
	B	0.83	0.82–0.84	0.003	0.829–0.831
2011–2020	C	0.73	0.69–0.77	0.02	0.729–0.736
	D	0.73	0.70–0.74	0.005	0.724–0.727
2000–2020	E	0.81	0.78–0.86	0.013	0.809–0.814
	F	0.80	0.79–0.81	0.003	0.803–0.804

intrinsically less efficient at dissipating wave energy compared to dissipative, low-gradient profiles. At the similar way, a short distance to the depth of closure implies a narrow active zone with limited accommodation space for the sediment, in this context the profile becomes highly sensitive to sediment losses during high-energy events. The identification of Drift Class 4 as a key predictor further confirms that sectors subjected to divergent longshore transport are structurally predisposed to retreat, as sediment removal exceeds natural supply. Finally, the models prioritize the number of storms over cumulative energy. Physically, this suggests that storm clustering (frequency) is more critical than the magnitude of individual events, as recurrent storms prevent the coastline from recovering its equilibrium profile. However, a marked difference arises between the three time periods, while the 2000–2010 model (Fig. 7, green bars) built complex basis functions integrating geomorphological setting and wave climate variables, the model 2011–2020 (Fig. 7, red bars) used just five predictors, four of which controlled by wave climate conditions. Factors like the main longshore sediment transport direction (D_r) or specific geomorphological classes (G), which contributed to the model in the first decade, exhibiting very high statistical significance ($p < 0.001$, Mann-Whitney Test), lost their statistical significance in the second period and were discarded during variable selection. This could suggest a transition in the coastal regime. In the 2000–2010 period, shoreline changes were driven by a balance

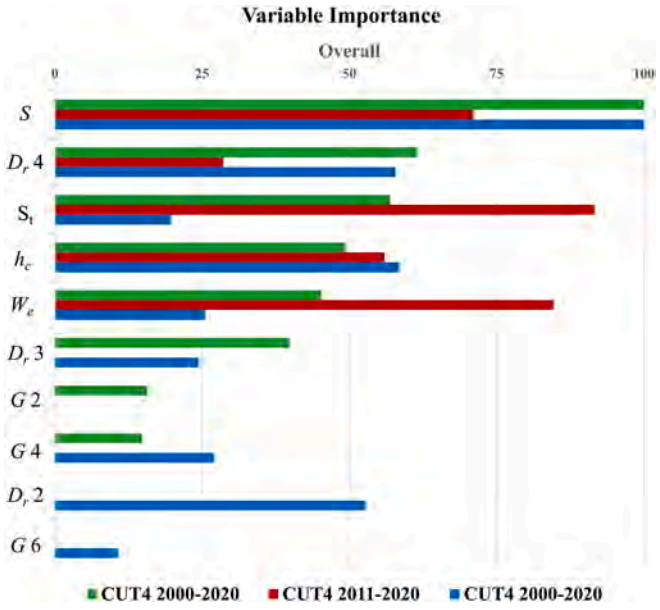

Fig. 7. Variable Importance plots for Models A, C, and E. The length of the bars indicates the strength of each variable's contribution to the models' predictive performance.

between the coast setting and wave energy. In the 2011–2020 period, the natural interaction between these factors – which MARS successfully modelled in the first decades – fades away. The model is not able to find stable basis functions involving geomorphological variables leaving only the wave climate variables as significant despite they create lower overall predictive accuracy. The analysis of the full 20-years period (Model E) shows an intermediate behaviour, with a mean AUC of 0.81 (Table 8) and a variable importance structure (Fig. 7, blue bars) similar to the 'natural' regime of the first decade. The Coastal Slope (S) is again

dominant (100% selection), and other predictors reappear, including the longshore sediment transport direction (D_r) and the geomorphological classes. The 2000–2020 model masks the weak predictive signal of the 2011–2020 period, demonstrating the importance of temporal division, in fact, using only the entire period would have led to the conclusion that the model is robust (AUC 0.81), losing the information that the system has changed in the recent decade. Once the importance of the predictors in determining the probability of erosion had been defined, these continuous probabilities generated by the model were converted into a binary classification. To identify the optimal cut-off threshold that maximized discrimination between stable and erosive sectors, the Youden Index criterion was applied, which is fundamental for deriving the final accuracy metrics (Sensitivity, Specificity, Accuracy). The Youden Index (J), applied to the ROC curves of the models, determines the optimal discrimination threshold. The Youden Index is defined as

$$J = \text{maximum}\ \{Sensitivity + Specificity - 1\}.$$

Geometrically, the maximum value of J is the maximum vertical distance between the ROC curve and the diagonal line (the line of no-discrimination) and indicates the cut-off point that ensures that the model correctly identify retreating transects (high sensitivity) and advancing transects (high specificity). In each ROC curves, the corresponding sensitivity and specificity for each threshold were used to calculate J. The threshold that produced the highest J value was selected as the optimal cut-off point. This method ensures that cut-off point used to binarize the prediction is chosen objectively, reflecting the best achievable discriminatory power for the specific model.

By applying the Youden-index criterion, optimal scores cut-off were recognized into the ROC-curve and a binarized prediction into advancing/retreating status produced for setting the confusion matrices (Table 9) which allow the evaluation of cut-off dependent accuracy metrics, including Sensitivity, Specificity, Positive Prediction Values (PPV), Negative Prediction Value (NPV). Model B (2000–2010), has the highest overall accuracy (0.76) and a sensitivity of 0.84. However, the value of specificity of 0.66 suggests a tendency to misclassify advancing transects as retreating. Model D (2011–2020), achieved the highest sensitivity (0.85), indicating a strong ability to correctly identify positive cases. However, it displayed the lowest performance among the three, with an accuracy of 0.69, a value of specificity of 0.50, and an overall accuracy of 0.69. A specificity of 0.50 implies that for advancing area, the model is guessing (50/50). The high sensitivity (0.85) is achieved only because the cut-off is low (0.43), this suggests that the optimization process was forced to lower the threshold significantly to capture the erosion signal, resulting in high value of false Positive and the lowest Overall Accuracy (0.69). Finally, Model F, had the highest specificity (0.81) and PPV (0.81), suggesting a strong capability in correctly classifying negative cases. However, its sensitivity was lower (0.60), resulting in a moderate overall accuracy of 0.73 and an NPV of 0.66.

To investigate whether the observed performance decline of Model D (2011–2020) was a consequence of human intervention, a temporal validation was conducted (model trained in the period 2000–2010, tested in the period 2011–2020, $n = 2244$ transects). An AUC of 0.58 was obtained, with high Sensitivity (0.94) but low Specificity (0.22). The high percentage of False Positive suggest that the rules learned during the calibration period (2000–2010) were not perfectly applicable to the second decade, likely due to latent factors not captured by the model—such as anthropogenic interventions (defence works or nourishment). To further test this, a temporal validation was performed again, dividing the dataset into two subsets: (1) transects affected by anthropogenic interventions during the 2010–2020 period, and (2) transects without direct interventions ('natural'). For transects affected by human interventions ($n = 929$), predictive performance decreased significantly, (Sensitivity 0.46 and AUC 0.58). The model misclassified 61% of these transects. In particular, in 25% of cases (False Positives), the model predicted erosion based on natural factors, but the coast remained stable; this suggests that interventions effectively mitigated the natural behaviour, masking the predicted erosion trend. Conversely, in 36% of cases (False Negatives), the model predicted stability, but the coast still retreated. This means that certain defence works were ineffective and also suggests that erosion was driven by interacting processes invisible to the model, such as sediment budget deficits or local erosion induced by the structures. In sectors without direct interventions ($n = 1315$ natural transects), the model shows high Sensitivity (0.89), it is able to correctly identify areas physically susceptible to erosion (AUC 0.63). However, the low Specificity (0.30) and the high percentage of False Positives (41%) indicate a overestimation of risk. This implies that the coastline exhibited a higher resilience than predicted by the 2000–2010 calibration.

4.3. Susceptibility map

In light of the obtained results, model F was adopted to depict the susceptibility spatial pattern of the Tuscany coast.

In fact, the marked difference in the performance of the 2011–2020 models (C and D) compared to the 2000–2010 models (A and B) suggest a structural discontinuity in the governing factors. This can be attributed to combined causes: on one hand, the anthropogenic pressures (nourishment and defence works) could have masked or amplified the erosion signal; on the other, there was a variation in the natural morphodynamic response which made the coastline more resistant in some sector. Further, although Model B (2000–2010) achieved the highest statistical accuracy, it was not selected because it is trained on an older regime, ignoring the recent human modifications and the new natural dynamics. Conversely, the 20-year models (E and F), have seen recent data and provide a comprehensive assessment of susceptibility that is more representative of the current reality. The final selection of the CUT2 criterion (Model F) over CUT4 (Model E) is based on negligible difference in their performance (AUC 0.80 and AUC 0.81, respectively). Although the CUT4 criterion is more rigorous, this minimal difference indicates that Model F (CUT2) maintains high predictive power; furthermore, this model allows a finer spatial resolution and continuous coverage.

Finally, for susceptibility mapping, minimizing False Positive is important to avoid overestimating risk. Model F achieved the highest Positive Prediction Value (0.81) and Specificity (0.81) among all models. This correspond to a conservative criterion, ensuring that the areas identify as susceptible are characterized by a very high probability of real erosion. Therefore, the model F (2000–2020 CUT 2) was selected for susceptibility mapping (Fig. 8).

In order to obtain four objective and quantitative susceptibility classes, a double recursive application of the Youden-index criterion was

Table 9
Performance metrics for models B, D, and F based on the optimal Youden Index cut-off. Metrics include overall accuracy, sensitivity, specificity, and predictive values (positive and negative.

Model	Youden Index Cut-off	Accuracy	Sensitivity	Specificity	Prediction value	
					Positive	Negative
B	0.46	0.76	0.84	0.66	0.75	0.77
D	0.43	0.69	0.85	0.50	0.66	0.75
F	0.59	0.73	0.60	0.81	0.81	0.66

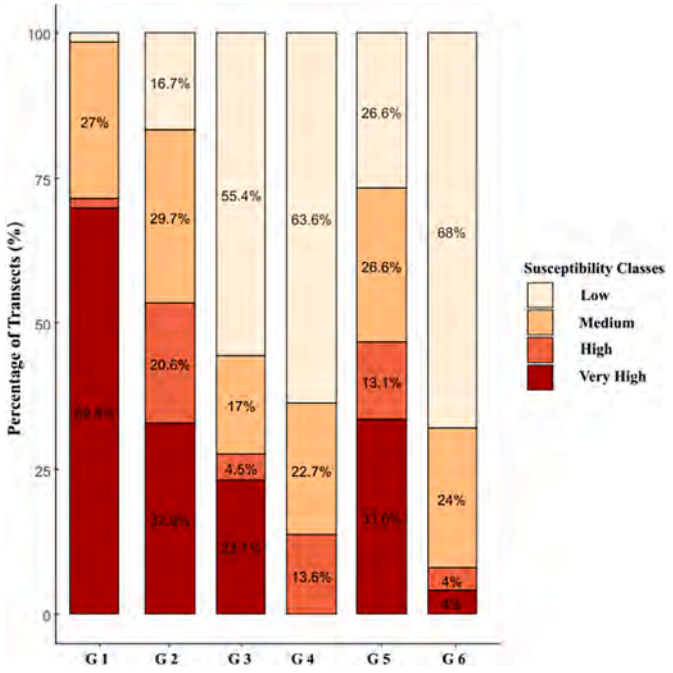

Fig. 8. The percentage distribution of susceptibility classes within each geomorphological class. (G1: Low Gravelly Coast; G2: Low Sandy Coast; G3: Low sandy coast with shifting or fixed dunes; G4: Connections; G5: Coastal Defence Structures; G6: Riverbanks). Susceptibility levels range from Low (beige) to Very High (dark red).

performed. The procedure consists of a two-step hierarchical classification. In the first level, the Youden Index was applied to the Model F (2000–2020) ROC curve, identifying the primary optimal cut-off at 0.59. This threshold split the dataset into two main subsets, RETREAT and ADVANCE (transects with score higher and lower than the cut -off value, respectively. In the second level, the Youden Index criterion was then re-applied independently to the specific ROC curves generated for each of these two subsets. This identified two secondary cut-offs, subdividing the ADVANCE subset into 1-Low and 2-Medium susceptibility, and the RETREAT subsets into 3-High and 4-Very High susceptibility. This approach generated four objectively defined susceptibility classes. The analysis of obtained susceptibility classes along the coast revealed that Class 4-Ver High susceptibility was the most prevalent (31.8%), followed by Class 2-Medium (27.4%) and Class 1-Low (23.7%). Class 3-High was the least represented, only 17.0% of the total transects fall within this class.

From the comparison of the susceptibility classes with the Geomorphology Classes (Fig. 8), emerges that Low Gravelly shorelines (G 1) are the more susceptible, with 69.8% of transects classified as "Very High." Low-Sandy Coasts (G 2) also show 32.9% of transects classified as "Very High." These coastlines consist of unconsolidated sediments (gravel and sand) highly dynamic and sensitive to wave energy. For sectors with Coastal Defence Structures (G 5), the percentage of transects falling into "Very High" susceptibility class (33.6%) could indicate the ineffectiveness of the structures, but likely reflects the fact that the hazard is still present.

Riverbanks (G 6) and Connections (G 4) appear to be the most stable classes. Riverbanks (G 6) shows the highest percentage of "Low" susceptibility (68%), with only a small fraction (4%) classified as "Very High." Connections (G 4) is the only geomorphological class where the "Very High" susceptibility class is missing; 63.6% of these transects are classified as "Low," followed by 22.7% as "Medium."

Finally, in the Low sandy coast with shifting or fixed dunes class (G 3) 55.4% of transects fall in the "Low" class and 23.1% are classified as "Very High," suggesting the presence of areas of erosion or instability within these costs.

By comparing the spatial distribution of the four susceptibility classes and the five associated consistent (2000–2020) NSM classes (NSM > 12 m; 12 m > NSM > 4 m; 4 m > NSM > -4 m; −4 m > NSM > -12 m; NSM < -12 m) transect responses (Fig. 9), it is confirmed the spatial correspondence of high/low susceptible to negative/positive (retreating/advancing) NSM transects, respectively.

The comparison between the Susceptibility Classes and the observed Net Shoreline Movement (NSM) values (Fig. 10a) attests for the high quality of the model, with a clear coherent median shifting toward retreating transects, from low (1) to very high (4) susceptibility classes. It is worth to note that the more marked separation arises for very low from medium susceptible transects, the former being characterized by strong advancing NSMs, and, to a lesser extent, for high from very high susceptible transects, the latter being characterized by strong retreating NSMs.

At the same time, a larger superimposition is observed between the medium and high susceptible transects. By analysing the results in the Susceptibility/NSM domain, a coherent trend from advancing to retreating transects is evident if moving from low to very high susceptible conditions Fig. 10.

By reclassifying the NSM values, a marked goodness of fit of the model more clearly arises (Fig. 10b). The majority of transects classified as having Low susceptibility (Class 1) match up to high shoreline advancement (NSM Class 1), while the transects with higher susceptibility classes (Classes 3 and 4) are pre- dominantly associated with greater shoreline retreat (NSM Classes 4 and 5). In particular, 82% of the transects classified as Very High Susceptibility (Class 4) fall into the two highest shoreline retreat classes (NSM Classes 4 and 5), corresponding to shoreline retreats greater than 4 m. As well, 62% of the transects classified as Low Susceptibility (Class 1) are associated with significant shoreline advancement (NSM Class 1).

Finally, Fig. 11 shows the relationship between the Susceptibility Classes derived from the model and the Coastline Dynamics Classes in the two periods considered. In facts, as above claimed, a large set of transects showed a reversal trend (i.e. "Advance → Retreat" and "Retreat → Advance"). A good correspondence is observed between the linear transects (i.e. "Advance → Advance" and "Retreat → Retreat") with strong concentration in the less (Classes 1 and 2) and more (Classes 3 and 4) susceptible classes. As expected, a less prediction skill of the model characterizes the reversal transects. This more scattered distribution could reflect the influence of local factors, temporal dynamics or anthropic interventions that the susceptibility model is not able to capture.

5. Discussion

The analysis of shoreline changes along the Tuscan coast between 2000 and 2021, as illustrated in Fig. 4, reveals a non-linear evolution of erosional and accretional patterns. The results show a predominance of erosional processes during the first decade (2000–2010), followed by a modest improvement in stability and localised accretion in the second (2011–2020), with the cumulative period reflecting the legacy of both dynamics. This temporal variation is not uniform across the region and reflects site-specific interactions be- tween sediment supply, coastal morphology, and anthropogenic pressures. In particular, near the Ombrone River (Fig. 4), exhibited severe shoreline retreat, consistent with previous studies that identified this delta as one of the most erosion-prone in the Italian peninsula. According to Cipriani et al. (2013), erosion rates in this sector can reach up to 5–6 m/year, driven by a combination of natural sediment starvation and human interventions such as up- stream dam construction. The persistence of erosional hotspots in Fig. 4-C2 underscores the ongoing vulnerability of this coastal system, even during periods of reduced retreat elsewhere. These trends are in line with findings from national-scale studies, which show that over 75% of Italian river deltas suffer from erosion, rising to 100% when

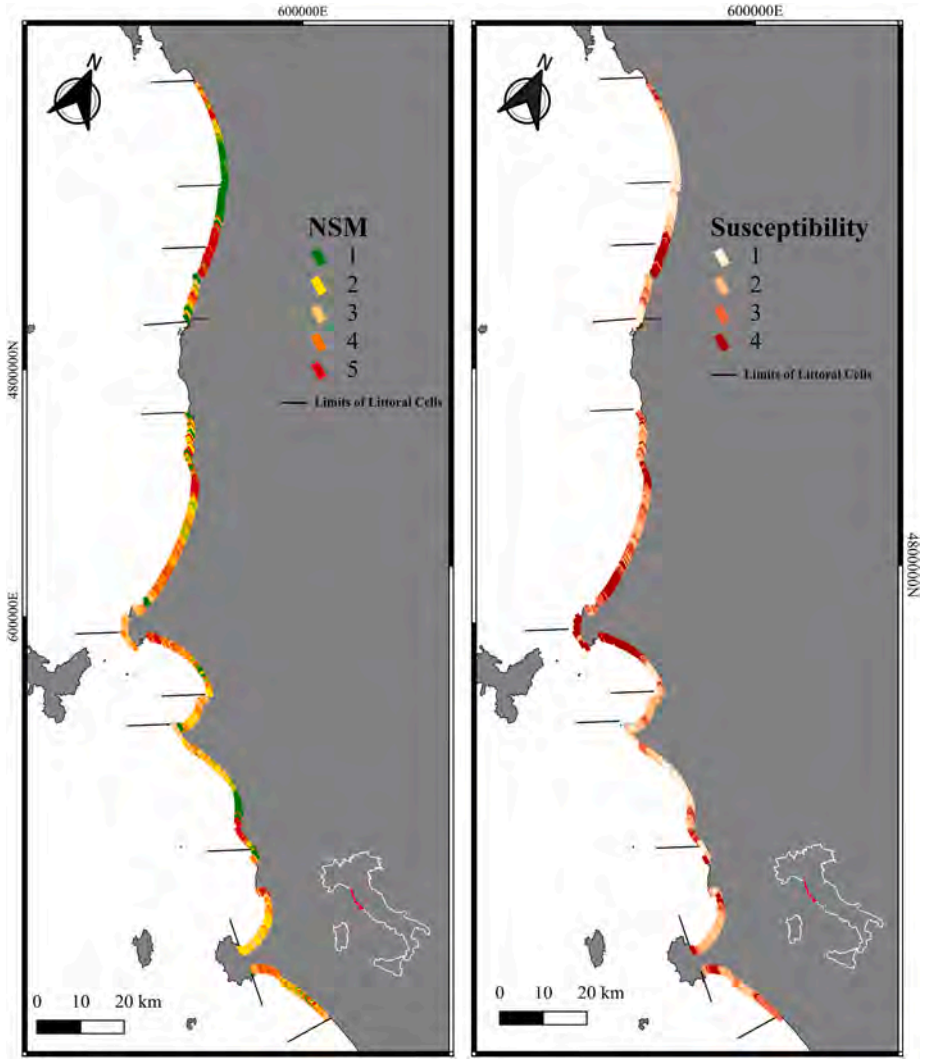

Fig. 9. Observed Net Shoreline Movement (left) and Predicted Susceptibility Classes from Model F (right) along the study area. Reference System: WGS84-UTM32N - EPSG:32632.

unprotected by hard infrastructure (Luppichini and Bini, 2025). The critical state of the Ombrone delta is strongly linked to long-term reductions in fluvial sediment input, due to both structural regulation (e.g., dams, levees) and hydroclimatic changes. The responses of the Ombrone delta reflect their distinct sediment budgets and coastal configurations. The Ombrone sector is affected by long-term sediment starvation linked to upstream regulation and reduced fluvial input.

Studies show that the Ombrone and Arno rivers have experienced a significant decline in suspended sediment transport over the past century, linked to decreasing precipitation, forest expansion, and land use changing across their catchments (Luppichini et al., 2024; Baronetti et al., 2022). These pressures have been shown to reduce not only the volume of sediments delivered to the coast but also the frequency of high-magnitude flood events capable of transporting coarse material to the shoreline. Although a recent moderate increase in events exceeding 700 m^3/s has been documented, values typically associated with sand transport, these have not been sufficient to reverse the erosion trends observed over the study period. On the contrary, the northern sector (Fig. 4, subsections A1–C1), which includes the urbanized areas of Viareggio and Marina di Massa, exhibited relatively stable or even increasing shoreline trends throughout the analysed period (2000–2020). However, some coastal stretches (e.g., Fig. 4, subplot A2) showed both advancing and retreating segments during the 2000–2010 period. This pattern shifted in the 2011–2020 period, with the emergence of erosive phenomena (e.g., Fig. 4, sub- plot B2). Therefore, when considering the entire analysis period (2000–2020), the shoreline's overall behaviour can be classified as erosive (e.g., Fig. 4, subplot C2). This observation aligns with recent findings that suggest shoreline stability in anthropized contexts often depends on continual human maintenance, including beach nourishment and artificial structures (Bini et al., 2021). In heavily urbanized and engineered stretches, such as that north of the Arno delta, the evolution of the shoreline is closely tied to direct human intervention. Indeed, the Pisa coastal plain has undergone intensive modifications since the early 20th century, with complex systems of groins and detached breakwaters constructed to counteract erosion (Bini et al., 2021; Pratellesi et al., 2018). Despite these defences, sediment dispersion studies using Sentinel-2 imagery show that a significant portion of riverine sediments is diverted offshore due to hydrodynamic shadowing and the orientation of jetty systems, particularly at the Arno mouth (Bini et al., 2021). This offshore loss of sediment, combined with the lack of consistent bypassing, explains why certain sectors continue to exhibit erosion or require constant artificial nourishment to maintain beach volumes. For example, areas south of Marina di Pisa and around Tirrenia have undergone repeated beach replenishment efforts over the last two decades (Bini et al., 2021) yet remain morphodynamically unstable. Marina di Pisa is strongly conditioned by hydrodynamic shadowing induced by jetties and coastal structures that divert the Arno sediment plume offshore. Fig. 12 shows

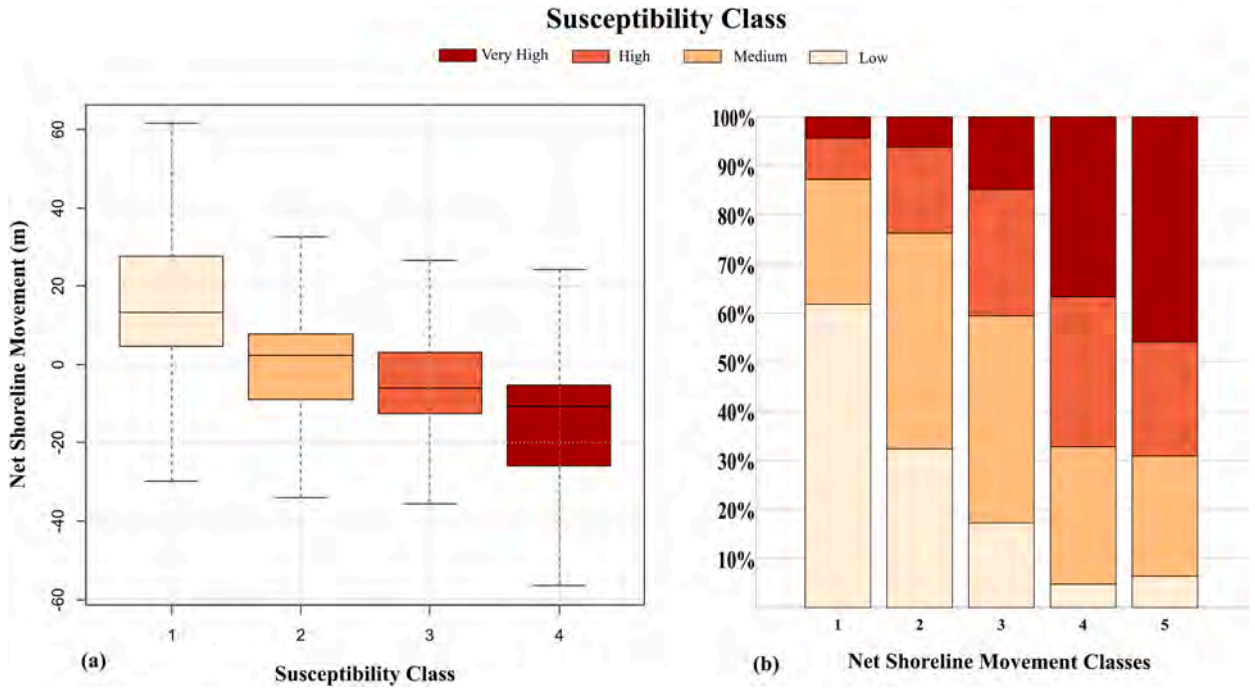

Fig. 10. a) Boxplot showing the distribution of observed Net Shoreline Movement (NSM) values across the four predicted Susceptibility Classes; b) Stacked bar plot showing the proportion of susceptibility classes predicted by Model F across different observed NSM classes.

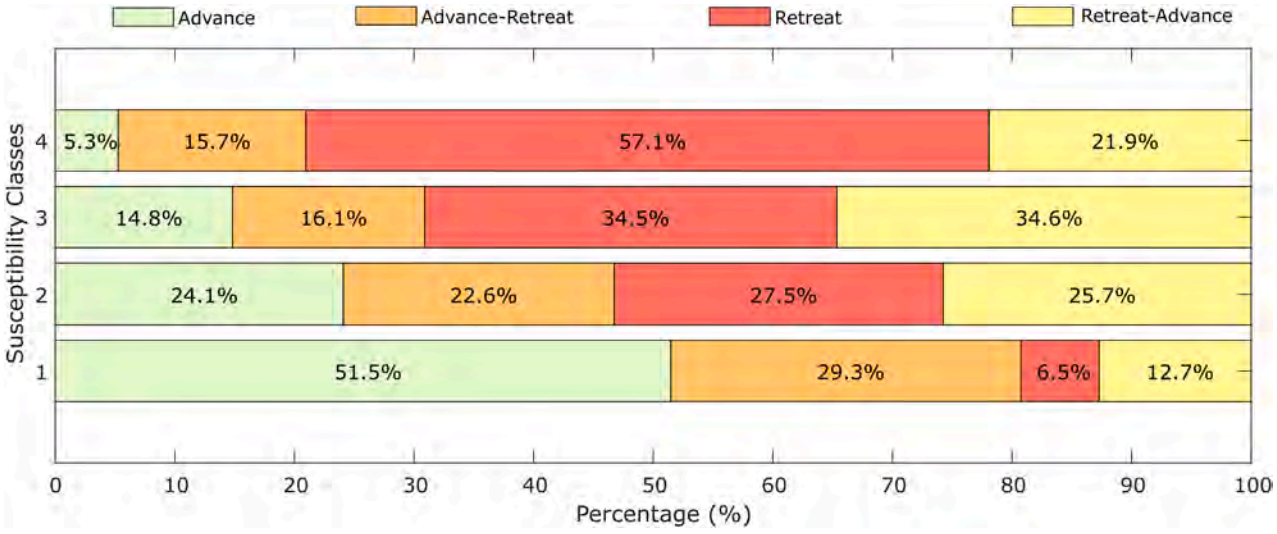

Fig. 11. Barplot showing the relationship between Susceptibility Classes predicted by the model (y-axis) and observed coastline dynamics classes (x-axis), where "Advance" indicates transects in advancement for both periods (2000–2010 and 2011–2020), "Retreat" refers to retreating transects, "Advance- > Retreat" represents transects that shifted from advancing to retreating, and "Retreat -> Advance" indicates the opposite trend.

four zoomed-in views of selected coastal segments. The dashed black line represents the shoreline position in 2000, while the solid black line corresponds to the shoreline in 2020. The susceptibility predicted by the model is symbolised by arrows, white arrows indicate low susceptibility, and dark red arrows indicate very high susceptibility. Starting from the northern part of the shoreline, in the 'Marina di Pietrasanta' sector, the agreement between observed shoreline evolution and predicted susceptibility is evident. This area experienced shoreline advancement during both periods, and the model correctly classified it as low susceptibility area. Similarly, the 'Marina di Pisa' sector, which under- went retreat in both periods, was classified as a very high susceptibility area. Moving toward the south of the Tuscany shoreline, near the Ombrone river, the agreement between the observed shoreline dynamic and the outcome of the model is still appreciable. However, the variable behaviour presents in these shoreline sectors- advance →retreat or retreat → advance- makes the model more challenging to maintain accuracy. These patterns align with recent Mediterranean studies reporting an acceleration of regional sea-level rise (Calafat et al., 2022) and an increase in storminess during the last two decades (Lionello et al., 2017). Regional analyses indicate that mean Mediterranean Sea-level rise accelerated to ~3.6 mm yr^{-1} in the early 21st century (De Leo et al., 2021) and that western Mediterranean sectors have experienced increasing storm intensity/wave energy (Amarouche et al., 2022; Amarouche and Akpınar, 2021), factors that can amplify shoreline retreat when coupled with sediment deficit. Although attribution to climate is beyond the scope of this retrospective analysis, these broader

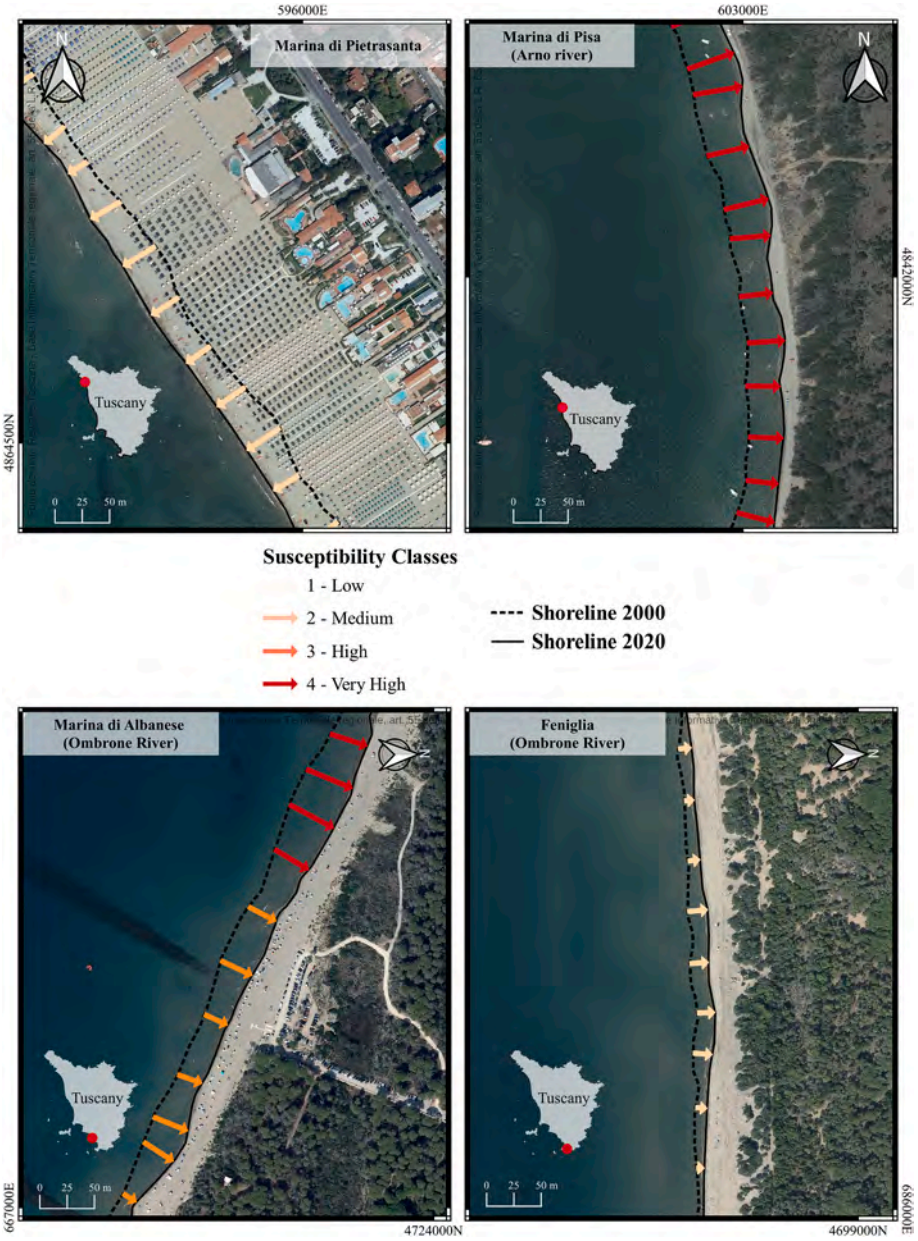

Fig. 12. Zoomed-in view of coastal segment. Reference System: WGS84-UTM32N - EPSG:32632.

trends are consistent with the spatial patterns of increased susceptibility identified in Tuscany. Although the present study is retrospective, the identified role of storm-related predictors suggests that projected increases in storm frequency and intensity could further enhance erosion susceptibility in the coming decades. Finally, the sediment-starved behaviour observed in some Tuscan deltaic sectors (e.g., Ombrone, parts of the Arno plume) are comparable to other Mediterranean deltas that have experienced marked sediment reductions due to river regulation and flow alteration. For example, the Rhône delta has been subject to significant morphodynamic changes (Fanget et al., 2016) linked to anthropogenic interventions and altered sediment delivery (Provansal et al., 2014); the Nile delta experienced accelerated erosion after the construction of the Aswan High Dam due to trapped sediment (Ghoneim et al., 2015). Similarly, the Ebro delta shows strong sediment deficit related to upstream abstractions and dams (Martin-Carrasco et al., 2025).

As regards the adopted methodology, a confirming picture has been obtained with an effective skill of the MARS modelling approach to explain the shoreline movements with a resolution up to ±2 m as the result of a set of explanatory variables whose informative layers can be easily gathered from a public repository for any region of Italy. In facts, differently from expert-based index-based approaches stochastic modelling allows to quantitatively and objectively detect importance and parameters of each single factor, as well as any potential collinearity between different factors, final multivariate score for shoreline response prediction, criteria for splitting into operative classes of the prediction scenarios and related maps.

Indeed, one of the more important steps in the modelling procedure is the selection of suitable analysis/mapping units, which have to correspond as far as possible to laterally closed systems, limiting the sediment transfer to adjacent units. At the same time, handling temporal shoreline movements databases allows the user to detect both temporal coherent and incoherent trends, opening the interpretation to the temporal changes in the controlling factors: mainly, wave climate and anthropogenic phenomena.

The results of the application of the MARS models underline the role

that physical and climatic variables play in the processes of coastline retreat and advance. Specifically, the slope of the coastline appears to be the most influential factor in both the 2000–2010 and 2000–2020 models. On the contrary, for the period 2011–2020, the variables associated with meteorological-marine conditions emerges as the most relevant predictors. Despite the overall good performance of the models (AUC greater than 0.7), in the period 2011–2020 a decrease in model accuracy and greater variability was observed. This could reflect a greater complexity of coastal dynamics in the last decade, potentially due to the combined and non-linear effects of climate, anthropogenic pressures and sediment transport processes. Overall, the results indicate that the model can identify with good reliability transects characterized by constant and coherent dynamics. However, the greater heterogeneity observed in transects with trend reversal suggests the need for future investigations or the integration of additional explanatory variables.

6. Conclusions

The observed evolution patterns confirm that Tuscan coastal systems are highly sensitive to both fluvial and marine forcing, and their future trajectory will largely depend on integrated watershed–coast approaches. A forward-looking strategy must integrate sediment flux restoration and nature-based solutions, in parallel with reassessing the effectiveness and un- intended consequences of hard defences. Restoration of sediment continuity along river systems—particularly in relation to dam management, floodplain reconnection, and improved monitoring of sediment transport—is essential to address the root causes of erosion. Moreover, adaptive coastal management must be informed by a detailed understanding of the temporal and spatial variability in shoreline response, including the role of hydrodynamics, sediment budgets, and human infrastructure. Without addressing the causes of sediment deficit, even the best coastal protection efforts risk being temporary, spatially limited, or even counterproductive.

As regards the specific experimental case, MARS modelling allowed to correctly predict the temporal evolution of the shoreline with a calibration to validation scheme both for each single time window and the whole period, attesting for the good accuracy and reliability of the method. However, some decreasing in the performance of the models arose for the 2011–2020 window as results of the lack of quantitative/qualitative data about anthropogenic subtraction (river damming) or supply (beach nourishment). At the same time, approaching coastal erosion susceptibility assessment by means of multivariate methods allow us to derive quantitative and objective estimation of the probability for any given coastal transect to extend/retreat from a reference baseline based on a set of predictors. Differently from largely adopted approaches, the proposed method dose not suffer for overfitting effects produced by the inclusion of the observed outcome signal among the controlling factors. In contrast, the past observed morphodynamic coastal signal is exploited to best fit the coefficients of the covariates which have been selected as potentially suitable to explain advancement/retreatment patterns. In particular, coastal slope (S), class 4 of the main longshore sediment transport direction (D_r4) and the variable related to wave climate are the most influencing for the model performance.

CRediT authorship contribution statement

Grazia Azzara: Writing – review & editing, Writing – original draft, Visualization, Validation, Software, Methodology, Investigation, Formal analysis, Data curation, Conceptualization. **Pietro Scala:** Writing – review & editing, Writing – original draft, Visualization, Validation, Software, Methodology, Investigation, Formal analysis, Data curation, Conceptualization. **Giorgio Manno:** Writing – review & editing, Writing – original draft, Validation, Methodology, Investigation, Data curation, Conceptualization. **Francesco Raffa:** Writing – review & editing, Writing – original draft, Methodology, Formal analysis, Data curation, Conceptualization. **Chiara Martinello:** Writing – review & editing, Methodology, Formal analysis, Data curation. **Antonio Tozzi:** Writing – review & editing, Writing – original draft, Methodology, Formal analysis, Data curation, Conceptualization. **Edoardo Rotigliano:** Writing – review & editing, Writing – original draft, Visualization, Validation, Supervision, Software, Methodology, Investigation, Formal analysis, Data curation, Conceptualization. **Giuseppe Ciraolo:** Writing – review & editing, Writing – original draft, Visualization, Validation, Supervision, Software, Methodology, Investigation, Formal analysis, Data curation, Conceptualization.

Declaration of competing interest

The authors declare the following financial interests/personal relationships which may be considered as potential competing interests: Giorgio Manno, Chiara Martinello, Edoardo Rotigliano reports financial support was provided by RETURN - European Union Next-GenerationEU (National Recovery and Resilience Plan). CUP B73C22001220006. If there are other authors, they declare that they have no known competing financial interests or personal relationships that could have appeared to influence the work reported in this paper.

Acknowledgments

This study was carried out within the RETURN Extended Partnership that received funding from the European Union Next-GenerationEU (National Recovery and Resilience Plan – NRRP, Mission 4, Component 2, Investment 1.3–D.D. 1243 2/8/2022, PE0000005). RETURN CUP B73C22001220006.

Data availability

Data will be made available on request.

References

Amarouche, K., Akpınar, A., 2021. Increasing trend on storm wave intensity in the western Mediterranean. Climate 9, 11. https://doi.org/10.3390/cli9010011.

Amarouche, K., Akpınar, A., Semedo, A., 2022. Wave storm events in the Western Mediterranean Sea over four decades. Ocean Model 170, 101933. https://doi.org/10.1016/j.ocemod.2021.101933.

Baronetti, A., Dubreuil, V., Provenzale, A., Fratianni, S., 2022. Future Droughts in Northern Italy: High-resolution Projections Using EURO-CORDEX and MED-CORDEX Ensembles 172, p. 22. https://doi.org/10.1007/s10584-022-03370-7.

Bayes, T., 1763. LII. An essay towards solving a problem in the doctrine of chances by the late rev. Mr. Bayes, Frs communicated by Mr. Price, in a letter to John Canton, Amfr s. Philos. Trans. R. Soc. Lond. 370–418.

Besset, M., Anthony, E., Sabatier, F., 2017. River delta shoreline reworking and erosion in the Mediterranean and Black Seas: the potential roles of fluvial sediment starvation and other factors. Elementa Sci. Anthropocene 5, 54. https://doi.org/10.1525/elementa.139.

Beuzen, T., Goldstein, E.B., Splinter, K.D., 2019. Ensemble models from machine learning: an example of wave runup and coastal dune erosion. Nat. Hazards Earth Syst. Sci. 19, 2295–2309. https://doi.org/10.5194/nhess-19-2295-2019.

Bini, M., 2008. L'evoluzione diacronica della linea di riva del litorale pisano (1938–2004) sulla base del confronto di immagini aeree georeferenziate, 113, 1–12.

Bini, M., Casarosa, N., Luppichini, M., 2021. Exploring the relationship between river dis- charge and coastal erosion: an integrated approach applied to the Pisa Coastal Plain (Italy). Remote Sens. 13, 226. https://doi.org/10.3390/rs13020226 publisher: MDPI AG.

Blöschl, G., Hall, J., Viglione, A., Perdigão, R.A.P., Parajka, J., Merz, B., Lun, D., Arheimer, B., Aronica, G.T., Bilibashi, A., Boháč, M., Bonacci, O., Borga, M., Čanjevac, I., Castel-larin, A., Chirico, G.B., Claps, P., Frolova, N., Ganora, D., Gorbachova, L., Gül, A., Hannaford, J., Harrigan, S., Kireeva, M., Kiss, A., Kjeldsen, T.R., Kohnová, S., Koskela, J.J., Ledvinka, O., Macdonald, N., Mavrova-Guirguinova, M., Mediero, L., Merz, R., Mol-nar, P., Montanari, A., Murphy, C., Osuch, M., Ovcharuk, V., Radevski, I., Salinas, J.L., Sauquet, E., Sraj, M., Szolgay, J., Volpi, E., Wilson, D., Zaimi, K., Živković, N., 2019. Changing climate both increases and decreases European river floods, 573, 108–111. https://doi.org/10.1038/s41586-019-1495-6.

Boccotti, P., 2000. Wave Mechanics for Ocean Engineering, Vol 64. Elsevier.

Burke, L., Kura, Y., Kassem, K., Revenga, C., Spalding, M., McAllister, D., Caddy, J., 2001. Coastal Ecosystems. World Resources Institute, Washington, DC. ISBN: 1-56973-458-5. http://pdf.wri.org/page_coastal.pdf.

Calafat, F.M., Frederikse, T., Horsburgh, K., 2022. The sources of sea-level changes in the Mediterranean Sea since 1960. J. Geophys. Res. Oceans 127, e2022JC019061. https://doi.org/10.1029/2022JC019061.
Cavazza, S., 1984. Regionalizzazione geomorfologica del trasporto solido in sospensione dei corsi d'acqua tra il Magra e Ombrone. Atti Soc. Tosc. Sci. Nat. Pisa, Mem. 119–132. ISSN 0365-7655. http://www.stsn.it/en/atti-memorie-serie-a/13-stsn/86-memorie-serie-a-anno-1984.html.
Cipriani, L., Pranzini, E., Vitale, G., Wetzel, L., 2013. Adaptation to beach erosion at Maremma regional park (Tuscany, Italy), 19, 65–75. https://doi.org/10.5281/zenodo.56844.
Conoscenti, C., Agnesi, V., Cama, M., Caraballo-Arias, N.A., Rotigliano, E., 2018. Assessment of gully erosion susceptibility using multivariate adaptive regression splines and accounting for terrain connectivity, 29, 724–736. https://doi.org/10.1002/ldr.2772.
De Leo, F., Besio, G., Mentaschi, L., 2021. Trends and variability of ocean waves under RCP8.5 emission scenario in the Mediterranean Sea. Ocean Dyn. 71, 97–117. https://doi.org/10.1007/s10236-020-01419-8.
EUROSION, 2004. A guide to coastal erosion management practices in Europe. Contract B4–3301/2001/329175/MAR/B3. Prepared by Rijkswaterstaat/RIKZ. https://repository.tudelft.nl/record/uuid:ec220e2c-0dec-440a-b17a-fde42135f4b3.
Fanget, A.-S., Bassetti, M.-A., Fontanier, C., Tudryn, A., Berné, S., 2016. Sedimentary Archives of Climate and Sea-level Changes During the Holocene in the Rhone Prodelta (NW Mediterranean Sea). https://doi.org/10.5194/cp-2016-57.
Frangipane, A., Paris, E., 1994. Long-term Variability of Sediment Transport in the Ombrone River Basin (Italy) Proceedings of the Canberra Symposium.
Friedman, 1991. Multivariate adaptive regression splines, 19, 1–67. https://doi.org/10.1214/aos/1176347963.
Ghoneim, E., Mashaly, J., Gamble, D., Halls, J., AbuBakr, M., 2015. Nile Delta exhibited a spatial reversal in the rates of shoreline retreat on the Rosetta promontory comparing pre- and post-beach protection. Geomorphology 228, 1–14. https://doi.org/10.1016/j.geomorph.2014.08.021.
Gornitz, V., 1991. Global coastal hazards from future sea level rise. Palaeogeogr. Palaeoclimatol. Palaeoecol. 89, 379–398. https://doi.org/10.1016/0031-0182(91)90173-O.
Gutierrez, B.T., Plant, N.G., Thieler, E.R., 2011. A Bayesian network to predict coastal vulnerability to sea level rise. J. Geophys. Res. Earth Surf. 116. https://doi.org/10.1029/2010JF001891.
Hosmer, D., Lemeshow, S., Sturdivant, R., 2013. Applied Logistic Regression. In: Wiley Series in Probability and Statistics. Wiley. URL: https://books.google.it/books?id=64JYAwAAQBAJ.
Lasko, T.A., Bhagwat, J.G., Zou, K.H., Ohno-Machado, L., 2005. The use of receiver operating characteristic curves in biomedical informatics, 38, 404–415. https://doi.org/10.1016/j.jbi.2005.02.008.
Lionello, P., Özsoy, E., Planton, S., Zanchetta, G., 2017. Climate variability and change in the Mediterranean Region. Glob. Planet. Chang. 151, 1–3. https://doi.org/10.1016/j.gloplacha.2017.04.005.
Luppichini, M., Bini, M., 2025. 40-year shoreline evolution in Italy: critical challenges in river delta regions. Estuar. Coast. Shelf Sci. 315, 109166. https://doi.org/10.1016/j.ecss.2025.109166.
Luppichini, M., Bini, M., Giannecchini, R., Zanchetta, G., 2023. High-resolution spatial analysis of temperature influence on the rainfall regime and extreme precipitation events in north-central Italy. Sci. Total Environ. 880, 163368. https://doi.org/10.1016/j.scitotenv.2023.163368.
Luppichini, M., Lazzarotti, M., Bini, M., 2024. Climate change as main driver of centennial decline in river sediment transport across the Mediterranean region. J. Hydrol. 636, 131266. https://doi.org/10.1016/j.jhydrol.2024.131266 publisher: Elsevier BV.
Martin-Carrasco, F., Santillán, D., López-Gómez, D., Iglesias, A., Garrote, L., 2025. Sediment transport constraints for restoration of the Ebro Delta. Water 17, 1620. https://doi.org/10.3390/w17111620.
Martinello, C., Mercurio, C., Cappadonia, C., Hernández Martínez, M., Reyes Martínez, M.E., Rivera Ayala, J.Y., Conoscenti, C., Rotigliano, E., 2022. Investigating Limits in Exploiting Assembled Landslide Inventories for Calibrating Regional Susceptibility Models: A Test in Volcanic Areas of El Salvador 12. https://doi.org/10.3390/app12126151.
Martinello, C., Cappadonia, C., Rotigliano, E., 2023. Investigating the Effects of Cell Size in Statistical Landslide Susceptibility Modelling for Different Landslide Typologies: A Test in Central–Northern Sicily 13. https://doi.org/10.3390/app13021145.
Martínez, M., Intralawan, A., Vázquez, G., Pérez-Maqueo, O., Sutton, P., Land- grave, R., 2007. The coasts of our world: ecological, economic and social importance, 63, 254–272. https://doi.org/10.1016/j.ecolecon.2006.10.022.
Mendoza, e.T., Jiménez, J.a., 2005. Factors controlling vulnerability to storm impacts along the Catalonian coast. In: Coastal Engineering 2004: (In 4 Volumes). World Scientific, pp. 3087–3099.
Mentaschi, L., Vousdoukas, M.I., Pekel, J.F., Voukouvalas, E., Feyen, L., 2018. Global long- term observations of coastal erosion and accretion, 8, 12876. https://doi.org/10.1038/s41598-018-30904-w.
Mercurio, C., Martinello, C., Rotigliano, E., Argueta-Platero, A., Reyes-Martínez, M., Rivera-Ayala, J., Conoscenti, C., 2021. Mapping susceptibility to debris flows triggered by tropical storms: a case study of the San Vicente Volcano area (El Salvador, CA). Earth 2, 66–85. URL: https://www.scopus.com/inward/record.uri?eid=2-s2.085132571851&doi=10.3390%2fearth2010005&partnerID=40&md5=02d6c77241979f8a25891e238617d337 https://doi.org/10.3390/earth2010005.
Novi, L., Salvatore, M.C., Raffa, F., Biasci, F., Provenzale, A., Baroni, C., 2022. Zonation of wave-induced erosion threat of a sandy shoreline in central Tuscany (Italy). Geogr. Fis. Din. Quat. 45, 185–195. https://doi.org/10.4461/GFDQ.2022.45.7.
Park, S.J., Achmad, A.R., Syifa, M., Lee, C.W., 2019. Machine learning application for coastal area change detection in Gangwon province, South Korea using high-resolution satellite imagery. J. Coast. Res. 90, 228–235. https://doi.org/10.2112/SI90-028.1 arXiv. https://meridian.allenpress.com/jcr/article-pdf/90/SI/228/2428964/si 0-0281.pdf.
Pearl, J., 2001. Bayesian Networks, Causal Inference and Knowledge Discovery. UCLA Cognitive Systems Laboratory, Technical Report. https://bayes.cs.ucla.edu/csl_papers.html.
Pranzini, E., Williams, A.T., 2021. The equilibrium concept, or. . . (mis)concept in beaches. Geosciences 11, 59. https://doi.org/10.3390/geosciences11020059.
Pranzini, E., Anfuso, G., Cinelli, I., Piccardi, M., Vitale, G., 2018. Shore protection structures increase and evolution on the northern Tuscany coast (Italy): influence of tourism industry. Water 10, 1647. https://doi.org/10.3390/w10111647.
Pranzini, E., Cinelli, I., Cipriani, L.E., Anfuso, G., 2020. An integrated coastal sediment management plan: the example of the Tuscany region (Italy). J. Mar. Sci. Eng. 8, 33. https://doi.org/10.3390/jmse8010033.
Pratellesi, M., Ciavola, P., Ivaldi, R., Anthony, E.J., Armaroli, C., 2018. River-mouth Geomorphological Changes Over >130 Years (1882–2014) in a Small Mediterranean Delta: Is the Magra Delta Reverting to an Estuary?, 403, pp. 215–224. URL: https://www.sciencedirect.com/science/article/pii/S0025322717304097 https://doi.org/10.1016/j.margeo.2018.06.003.
Provansal, M., Dufour, S., Sabatier, F., Anthony, E.J., Raccasi, G., Robresco, S., 2014. The geomorphic evolution and sediment balance of the lower Rhône River (southern France) over the last 130 years: hydropower dams versus other control factors. Geomorphology 219, 27–41. https://doi.org/10.1016/j.geomorph.2014.04.033.
Raffa, F., Alberico, I., Serafino, F., 2022. X-band Radar System to Detect Bathymetric Changes at River Mouths During Storm Surges: A Case Study of the Arno River, 22, p. 9415. https://doi.org/10.3390/s22239415.
Rangel-Buitrago, N., Anfuso, G., 2015. Introduction. Springer International Publishing, Cham, pp. 1–5. https://doi.org/10.1007/978-3-319-15844-0_1.
Rinaldi, M., 2003. Recent channel adjustments in alluvial rivers of Tuscany, central Italy. Earth Surf. Process. Landf. 28, 587–608 doi:10.1002/esp.464. publisher: Wiley.
Scala, P., Manno, G., Ciraolo, G., 2024a. Coastal Dynamics Analyser (CDA): A QGIS Plugin for Transect Based Analysis of Coastal Erosion, 28, p. 101894. https://doi.org/10.1016/j.softx.2024.101894. https://www.sciencedirect.com/science/article/pii/S2352711024002644.
Scala, P., Manno, G., Ciraolo, G., 2024b. Semantic segmentation of coastal aerial/satellite images using deep learning techniques: an application to coastline detection. Comput. Geosci. 192. https://doi.org/10.1016/j.cageo.2024.105704.
Stocker, T., Qin, D., 2013. Climate Change 2013: The Physical Science Basis: Summary for Policymakers, a Report of Working Group of the IPCC: Technical Summary, a Report Accepted by Working Group of the IPCC but not Approved in Detail: and Frequently Asked Questions: Part of the Working Group Contribution to the Fifth Assessment Report of the Intergovernmental Panel on Climate Change. https://www.ipcc.ch/report/ar5/wg1/.
Torresan, S., Critto, A., Rizzi, J., Zabeo, A., Furlan, E., Marcomini, A., 2016. Desyco: a decision support system for the regional risk assessment of climate change impacts in coastal zones. Ocean Coast. Manag. 120, 49–63. https://doi.org/10.1016/j.ocecoaman.2015.11.003.
Tursi, M.F., Anfuso, G., Manno, G., Mattei, G., Aucelli, P.P.C., 2025. A multi component approach to predict erosion susceptibility of rocky coasts: marine, terrestrial and climatic forcing—an application in southern Italy, 84, 183. https://doi.org/10.1007/s12665-025-12143-1.
Youden, W.J., 1950. Index for rating diagnostic tests, 3, 32–35. https://doi.org/10.1002/1097-0142(1950)3:1<32::AID-CNCR2820030106>3.0.CO;2-3.